

A Survey for Planetary Nebulae in M31 Globular Clusters

George H. Jacoby

*Giant Magellan Telescope / Carnegie Observatories, 813 Santa Barbara Street, Pasadena,
CA 91101*

gjacoby@gmto.org

Robin Ciardullo

*Department of Astronomy & Astrophysics, The Pennsylvania State University, University
Park, PA 16802*

rbc@astro.psu.edu

Orsola De Marco

Department of Physics & Astronomy, Macquarie University, Sydney, NSW 2109, Australia

orsola.demarco@mq.edu.au

Myung Gyoon Lee

*Astronomy Program, Department of Physics and Astronomy, Seoul National University,
Seoul 151-742, Korea*

mglee@astrog.snu.ac.kr

Kimberly A. Herrmann

Lowell Observatory, Flagstaff, AZ 86001

herrmann@lowell.edu

Ho Seong Hwang

Smithsonian Astrophysical Observatory, 60 Garden Street, Cambridge, MA 02138

hhwang@cfa.harvard.edu

Evan Kaplan

Vassar College, 124 Raymond Ave., Poughkeepsie, NY 12604

evanskaplan@gmail.com

and

James E. Davies

Smithsonian Astrophysical Observatory, 60 Garden Street, Cambridge, MA 02138

jdavies@cfa.harvard.edu

ABSTRACT

We report the results of an [O III] $\lambda 5007$ spectroscopic survey for planetary nebulae (PNe) located within the star clusters of M31. By examining $R \sim 5000$ spectra taken with the WIYN+Hydra spectrograph, we identify 3 PN candidates in a sample of 274 likely globular clusters, 2 candidates in objects which may be globular clusters, and 5 candidates in a set of 85 younger systems. The possible PNe are all faint, between ~ 2.5 and ~ 6.8 mag down the PN luminosity function, and, partly as a consequence of our selection criteria, have high excitation, with [O III] $\lambda 5007$ to $H\beta$ ratios ranging from 2 to $\gtrsim 12$. We discuss the individual candidates, their likelihood of cluster membership, and the possibility that they were formed via binary interactions within the clusters. Our data are consistent with the suggestion that PN formation within globular clusters correlates with binary encounter frequency, though, due to the small numbers and large uncertainties in the candidate list, this study does not provide sufficient evidence to confirm the hypothesis.

Subject headings: planetary nebulae: general — globular clusters: general — galaxies: individual (M31) — stars: evolution

1. Introduction

Despite over a century of observations and decades of detailed modeling, the stellar population that forms planetary nebulae (PNe) is still somewhat of a mystery. The traditional theory states that the progenitors of PNe are low- to intermediate-mass single stars at the end of the AGB phase (Shklovski 1956; Abell & Goldreich 1966). This hypothesis explains the distribution of PNe throughout space, and is responsible for the widely-held belief that the Sun will eventually evolve through this easily identifiable nebular phase (e.g., Abell & Goldreich 1966; Ciardullo et al. 1989; Buzzoni et al. 2006). However, this theory does not provide a natural explanation for the non-spherical morphologies observed for the

great majority of PNe, nor their low rate of formation. For these and other inconsistencies (see De Marco 2009), a new paradigm has been developed, wherein most planetary nebulae are shaped via the interaction of an AGB wind with a binary companion (e.g., Soker 1997).

Unfortunately, while the binary interaction model explains some of the anomalies associated with the observed planetary nebula population (Moe & De Marco 2006; De Marco 2009; Moe & De Marco 2012), this theory awaits final confirmation: the number of PN central stars with known binary companions is still relatively small, and programs to detect such objects are extremely challenging (De Marco et al. 2011, 2012). Moreover, neither the single-star nor binary-star hypothesis can explain the luminosities observed for PNe in the old stellar populations of elliptical galaxies and spiral bulges (Ciardullo et al. 2005), nor the invariance of the bright end of the planetary nebula luminosity function (PNLF) across stellar populations (Ciardullo et al. 2002). For this, one must invoke yet another formation scenario, wherein significant mass transfer (or a complete stellar merger) occurs prior to the planetary nebula phase (Ciardullo et al. 2005; Soker 2006).

It is difficult to probe the different PN formation scenarios using field stars, since one has almost no prior information about the properties of the PN progenitors. However, within star clusters, the situation is different, as both the age and metallicity of the progenitor can be accessed. Moreover, the low turnoff mass of old globular clusters (GCs) provides a tool with which to probe the binary formation scenario directly. Because GCs generally have turnoff masses less than $1M_{\odot}$, any post-AGB core arising from simple single-star stellar evolution must have a very small mass, $M_{\text{core}} \lesssim 0.54M_{\odot}$ (Kalirai et al. 2008), and an extremely long evolutionary timescale, $t > 10^5$ yr (e.g., Caloi 1989). Such objects cannot make planetary nebulae by themselves, since the mass lost during the AGB phase will disperse long before the core becomes hot enough to generate ionizing radiation. Any PN detected in these systems must therefore come from an alternate evolutionary channel, such as a common-envelope interaction or a mass augmentation process (i.e., a stellar merger).

Searches for planetary nebulae in Galactic clusters have turned up only a few associated objects. Although more than a dozen PNe are projected near open clusters, the vast majority are undoubtedly line-of-sight coincidences (Majaess et al. 2007; Parker et al. 2011). Similarly, out of 130 Galactic GCs surveyed, only four host PNe: Ps 1 in M15 (Pease 1928), GJJC-1 in M22 (Gillett et al. 1986), JaFu1 in Pal 6, and JaFu2 in NGC 6441 (Jacoby et al. 1997). Two of these PNe have high mass central stars more appropriate to PNe within open clusters ($\sim 0.62 M_{\odot}$ for Ps 1 and $\sim 0.75 M_{\odot}$ for GJJC-1; Bianchi et al. 2001; Harrington & Platoglou 1993), while the others have highly non-spherical nebulae (De Marco 2011). (The true nature of GJJC-1 is currently being re-assessed due to its high stellar mass, low nebular mass, and bizarre chemical composition (Jacoby et al. 2013), but

for this paper, we adopt the usual PN classification.) These facts, along with the observation that three of the four PNe are located in clusters that are rich in X-ray sources, suggest that interacting binaries play a role in the formation of cluster PNe (Jacoby et al. 1997).

Since the sample of PNe within Galactic globular clusters is small, the significance of any conclusion based on their properties is low. To better understand the processes that form PNe within clusters, many more objects are required. For this, we must look to other galaxies. Unfortunately, while there have been a few isolated associations of [O III] $\lambda 5007$ emission with extragalactic globular clusters (Minniti & Rejkuba 2002; Bergond et al. 2006; Larsen 2008; Chomiuk et al. 2008), these discoveries have largely been serendipitous, and in most cases only sensitive to the most luminous planetary nebulae. Peacock et al. (2012) did conduct a systematic search for PNe within the massive globular clusters of the giant Virgo elliptical NGC 4472, but again, this survey (which did not find any objects) was only sensitive to objects in the top ~ 2.5 mag of the luminosity function. Since bright PNe are relatively rare, a deeper investigation is needed to place better constraints on the phenomenon.

Here we report the results of a spectroscopic survey for planetary nebulae within the star clusters of M31. In §2, we describe our multi-fiber observations and the basic reduction steps needed to analyze ~ 460 candidate star clusters in M31. In §3, we describe our search for embedded planetary nebulae, and the techniques required to recover objects that are more than ~ 6 mag down the planetary nebula luminosity function. We present a list of the clusters surveyed, along with their magnitudes and radial velocities, and identify those clusters in which [O III] $\lambda 5007$ emission is present. In §4, we describe the individual PN candidates and their host clusters. Finally, we discuss our results, and show that the number of PNe recovered within M31’s globular cluster system is roughly consistent with surveys of Milky Way clusters.

2. Observations and Reductions

On 2008 Oct 25-28 (UT), we targeted 467 candidate star clusters in M31 with the 3.5-m WIYN telescope on Kitt Peak and the Hydra multi-fiber spectrograph. The objects selected for study were largely taken from a list of clusters given in the Revised Bologna Catalog (RBC; Galleti et al. 2004, 2007) and supplemented using the X-ray cluster identifications of Fan et al. (2005) and the young cluster candidates of Caldwell et al. (2009). As a control, we also positioned spare fibers on known M31 planetary nebulae taken from the list of Merrett et al. (2006). These PNe span a range of brightnesses, from $20.5 < m_{5007} < 25.9$ (i.e., $-13.71 > \log F_{5007} > -15.85$), and allowed us to test the depth of our exposures and the accuracy of our wavelength calibration. Finally, to estimate the background light and

the amount of diffuse [O III] emission arising from M31’s disk, several fibers in each setup were offset onto regions of blank sky.

Our specific target selections were made using the fiber-assignment program `whydra`. Since the M31 globular cluster system covers a much larger area than the 1° field-of-view of the WIYN+Hydra instrument (see Figure 1), we began by visualizing the locations of the individual clusters using the [O III] images of the Local Group Galaxies Survey (Massey et al. 2007). To accommodate the bulk of the galaxy’s cluster population, we located our first four setups on M31’s bulge. Thereafter, we alternated between regions southwest and northeast of the galactic center, each time allowing `whydra` to identify an optimal field position by searching a 25×25 grid of space in $0'.1$ increments, with 15 possible rotation angles (between 0° and 30°) at each location. Top priority for fiber assignments was always given to previously unobserved clusters, with duplicate clusters, field PNe, and blank sky positions assigned lesser precedence. In total, eight different setups were executed over the four nights of the observing run, and data were acquired for 391 RBC clusters, 64 X-ray clusters, and 12 young clusters, with 30 of the systems being targeted more than once. An additional 55 of M31’s field planetary nebulae were also observed. A log of the observations is given in Table 1.

To execute these observations, the WIYN+Hydra system was configured to use the instrument’s array of $3''$ diameter blue-sensitive fibers, the WIYN Bench spectrograph, and a $740 \text{ lines mm}^{-1}$ Volume Phase Holographic (VPH) grating designed to optimize throughput near 5000 \AA . The resultant spectra covered the wavelength range between 4400 \AA and 5450 \AA at 1 \AA resolution and $0.5 \text{ \AA pixel}^{-1}$. Typically, each Hydra setup was observed for 3.5 hr via a series of seven 30 minute exposures.

Our initial reduction procedures were similar to those described in Herrmann & Ciardullo (2009). We began with the tasks within the IRAF¹ `ccdred` package: the data were trimmed and bias-subtracted via `ccdproc`, dome flats (typically three per setup) were combined using `flatcombine`, and CuAr comparison arcs, which bracketed the program exposures, were combined via `imcombine`. Next, `dohydra` within the `hydra` package was used to combine and linearize the spectra, with the averaged dome flats serving to define the extraction apertures, and the averaged comparison arcs providing the wavelength calibration. We estimate these wavelength calibrations to be precise to 0.04 \AA yielding 1σ errors of $\sim 2.4 \text{ km s}^{-1}$. As we illustrate below, this is small in comparison with the other uncertainties associated with our radial velocity determinations.

¹IRAF is distributed by the National Optical Astronomy Observatory, which is operated by the Association of Universities for Research in Astronomy (AURA) under cooperative agreement with the National Science Foundation.

After extracting each spectrum, the program objects were sky subtracted using the data acquired through our blank-field fibers. This step was straightforward: since all the data were taken in dark time and no bright sky lines fell within the wavelength range of the instrument, we simply used `scombine` to combine the extracted spectra from the multiple exposures and then invoked `skysub` to perform the subtraction. As will be explained in § 3, our searches for PN emission involved the subtraction of template spectra derived from the data themselves. Since these templates underwent the same sky subtraction, our procedure was differential in nature, and the details of sky subtraction had no significant effect on the analysis.

The final step in the basic data reduction involved estimating the response function of our instrument. Relative spectrophotometry across the entire spectral range of WIYN+Hydra was unnecessary for our program. Instead, we concentrated on determining the instrumental sensitivity at $H\beta$ and [O III] $\lambda 4959$ relative to [O III] $\lambda 5007$. The [O III] $\lambda 4959$ calibration was straightforward. Of the 55 planetary nebulae targeted via our spare fibers, all but one were recovered in [O III] $\lambda 5007$, and 51 out of 55 had detectable [O III] $\lambda 4959$. By comparing the observed ratio of the oxygen doublet to the astrophysical ratio of 2.92, we concluded that the spectroscopic throughput at 4959 Å was $\sim 90\%$ that at 5007 Å.

The procedure for estimating the instrumental response at $H\beta$ was slightly more complicated. We began by identifying 15 bright clusters and comparing their continuum flux near 5000 Å to that surrounding the $H\beta$ line. Spectral libraries (e.g., Jacoby et al. 1984) show that, after applying M31’s foreground reddening ($E(B - V) = 0.062$; Schlegel et al. 1998), the spectral energy distributions of old stellar populations should be flat between 4800 Å and 5100 Å. Consequently, to estimate the relative system response at $H\beta$, we simply adopted the inverse of the observed $\lambda 5007$ to $H\beta$ continuum ratio. Our estimate of 68% is slightly greater than the 62% value expected from the Bench spectrograph system and the VPH grating (Bershady et al. 2008). However, since the efficiency of this grating is only known to $\sim 10\%$, the two numbers are consistent.

Figure 2 compares the [O III] $\lambda 5007$ counts recorded in our PN spectra to the objects’ apparent magnitudes as determined by the counter-dispersed imaging of Merrett et al. (2006). There is a substantial amount of scatter in the diagram, due to the photometric and astrometric errors associated with the measurements from the Planetary Nebula Spectrograph, imperfections in our fiber positioning, and the effects of variable sky conditions. Nevertheless, the data demonstrate that our observations go quite deep: since we can detect emission lines containing as few as ~ 100 counts, our observations are sensitive to PNe that are ~ 6 mag down the luminosity function.

3. Finding PNe Within Star Clusters

Three criteria must be met before we can claim the detection of a PN candidate within an M31 star cluster. First, we must identify the presence of emission lines in the spectrum of the cluster. Second, the observed emission lines must have line-ratios consistent with those expected from a planetary nebula. Because of our limited spectral coverage (chosen to achieve the resolution needed to optimize emission line detections), this criterion is equivalent to requiring that the ratio of [O III] λ 5007 to $H\beta$ be greater than some threshold (see below). Third, the velocity of a PN candidate, as derived from its emission-lines, must be consistent with that of a star bound to its parent star cluster. Since the escape velocity from a typical M31 cluster is low, the precision of our emission-line and absorption line velocity measurements is an important parameter for our selection criteria.

3.1. Detection of Emission-lines

To search for PN emission within globular clusters, we began by normalizing each program spectrum with the `continuum` command within IRAF. We next divided the spectra into five classes based on the strengths and widths of the absorption features, thereby effectively grouping the clusters by age and metallicity. The highest signal-to-noise spectrum of each class was then chosen as a template, and shifted to zero velocity using, as a reference, the absorption lines of $H\beta$, the Mgb triplet ($\lambda\lambda$ 5167,5173,5184), and other strong features. The remaining clusters of the class were then cross-correlated against their template to determine their relative radial velocities, and shifted to the rest frame. Finally, to improve the detectability of any faint emission feature which may be lost amidst the background light, the template spectra were scaled and subtracted from the other members of their class. Figure 3 shows the five template spectra.

Figure 4 illustrates this template-subtracting procedure using the globular cluster B094-G156. This example is representative of our reductions; some of the template subtractions are much better, while others are poorer (see Section 4). In particular, because there were only five template clusters, not all the observed systems flattened as well as the one that is displayed. In particular, several of the clusters classified as “young” by Caldwell et al. (2009) had imperfect subtractions around $H\beta$. Nevertheless, in virtually all cases, the technique worked well around 5007 Å, as it effectively suppressed the continuum, allowing us to detect extremely weak emission from [O III]. Moreover, even when $H\beta$ was poorly subtracted, we could still measure the emission-line ratios extremely well, as the underlying stellar absorption was far broader than the unresolved Balmer emission.

3.2. The Emission-line Signature

Our next step was to look for evidence of planetary nebula emission. Because our data were taken using a multi-fiber spectrograph, rather than traditional slit spectroscopy, local sky subtraction was not possible. Consequently, the emission arising from the diffuse ionized gas of M31’s disk could not always be removed cleanly, and, even in the galactic bulge, line contamination was frequently a problem (see Ciardullo et al. 1988, for an image of M31’s bulge emission). In fact, as summarized in Table 3, roughly one-third of the globular clusters surveyed displayed some evidence of emission, due mostly to M31’s warm interstellar medium.

To guard against this form of false detection, we considered the expected line ratios of a planetary nebula. Most bright PNe are high excitation objects: in the top 2.5 mag of the [O III] PNLF, all planetary nebulae have [O III] $\lambda 5007$ to $H\alpha$ ratios greater than 3 (i.e., $I(\lambda 5007)/I(H\beta) \gtrsim 9$), and even at fainter magnitudes, [O III] $\lambda 5007$ is usually twice the strength of $H\beta$ (Ciardullo et al. 2002; Herrmann & Ciardullo 2009). In the metal-poor environments of globular clusters, this lower limit is even more appropriate: of the 11 halo and globular cluster PNe observed by Howard et al. (1997) and Jacoby et al. (1997), all have an excitation parameter, $R = I(\lambda 5007)/I(H\beta) > 2$. In contrast, the vast majority of M31’s H II regions and diffuse ionized emission have $H\beta$ brighter than [O III] $\lambda 5007$ (e.g., Blair et al. 1982; Galarza et al. 1999; Greenawalt et al. 1997). Moreover, in those rare cases where an H II region does exhibit a high value of R , its ionizing source (either a single O star or a very young OB association) must be very hot. Such an object will therefore be very luminous — more than 100 or 1000 times the brightness of a PN central star — and detectable either via its blue continuum or its overly bright emission-line luminosity.

The only other sources that may have an excitation similar to that of a PN are supernova remnants (SNRs), supersoft x-ray sources, and symbiotic stars. Supernova remnants are relatively rare (a factor of ~ 10 less numerous than PNe), and those remnants with $R > 2$ are less common still (Magnier et al. 1995; Galarza et al. 1999). If a SNR were embedded within one of our target clusters, it would likely be much brighter and/or have much broader emission lines than any PN. Supersoft x-ray sources are even rarer than SNRs, and most either have sizes much larger than a star cluster (Remillard et al. 1995) or are associated with classical novae (Pietsch et al. 2005). In this latter case, the nova ejecta would have a velocity structure that is easily resolvable in our $R \sim 5000$ spectra. Finally, symbiotic stars can produce high-excitation emission lines, and in some cases, their observed properties can be very similar to those of true PN (Frankowski & Soker 2009). In fact, Soker (2006) has argued that *all* the bright PNe seen in extragalactic surveys are actually symbiotic stars. But this is hard to prove, and PN surveys in the Milky Way and the LMC find that symbiotic

systems are only a minor contaminant (Viironen et al. 2009; Miszalski et al. 2011). Thus, emission-line sources that have [O III] $\lambda 5007$ more than twice the strength of H β are much more likely to be PNe than H II regions, SNRs, or some other line-emitting object.

Another way of testing for unrelated line emission is through the use of direct images. Deep H α and [O III] $\lambda 5007$ Mosaic CCD frames of a 2.2 deg² region along M31’s disk are available through the Local Group survey program of Massey et al. (2007). These images, which reach point-source flux limits of $\log F \sim -15.7$ in H α and $\log F \sim -15.5$ in [O III], can be used to examine the immediate environment of each cluster. Although not useful for weak emission, the frames provided a check for objects where the evidence for an associated PN was ambiguous.

3.3. Associating a PN Candidate with a Star Cluster

Even when high-excitation emission was detected in our fibers, its source was not always associated with the underlying globular cluster. Some of the emission within M31’s disk does have relatively high excitation, and there is always the possibility of a chance superposition of a cluster with a true but unassociated PN. We can quantify the latter likelihood by computing the probability that a field planetary nebula would be projected within 1’’5 of an M31 cluster entirely by chance. As in other galaxies, the distribution of M31 PNe closely follows that of the galactic light (Merrett et al. 2006), and, from the surface photometry of Kent (1987) and the bolometric corrections of Buzzoni et al. (2006), we calculate that $\sim 2 \times 10^7 L_{\odot}$ of M31’s diffuse luminosity (i.e., exclusive of the globular clusters) is projected within our survey fibers. This number, coupled with M31’s luminosity-specific PN density (Merrett et al. 2006), and the planetary nebula luminosity function (Ciardullo et al. 1989) implies the existence of ~ 0.4 superpositions in the top 2.5 mag of the PNLf, and ~ 3 unassociated PNe within the limits of our survey. Other high-excitation objects, such as old SNRs or supersoft X-ray sources will then increase this number. Clearly, we cannot ignore the possibility that two rather rare objects can be projected within a single optical fiber.

The best way to reject these chance superpositions is to compare the radial velocity of each cluster’s candidate PN to that of its stars. In general, for a planetary nebula to be bound to a cluster, the difference, Δv , between its emission-line radial velocity and the absorption-line radial velocity of the cluster’s stars should satisfy the criterion $\Delta v \lesssim 3\sigma_{\text{eff}}$, where σ_{eff} is the quadrature sum of the system’s internal velocity dispersion and the uncertainty in the radial velocity measurements. The former quantity exists for $\sim 60\%$ of the globular clusters in our survey, mostly through the $R \sim 34,000$ MMT echelle spectroscopy of Strader et al. (2011). For the remaining old stellar systems, we can estimate the line-of-sight velocity

dispersions through the clusters’ fundamental plane relation (e.g., Djorgovski et al. 1997; Strader et al. 2009, 2011). While we generally do not have access to information about a cluster’s size or surface brightness, a projection of the Strader et al. (2011) clusters onto the $M - \sigma$ plane yields

$$\sigma(\text{km s}^{-1}) \sim 23.5 + 8M_{T_1} + 0.7M_{T_1}^2 \quad (1)$$

where M_{T_1} is the cluster’s absolute T_1 magnitude in the Washington system (Kim et al. 2007), and σ is the observed velocity dispersion. Typically, these velocity dispersions span the range $3 \lesssim \sigma_0 \lesssim 30 \text{ km s}^{-1}$, with a median value near $\sim 8 \text{ km s}^{-1}$. Young clusters do not necessarily follow this relation, but from the structural analysis by Barmby et al. (2009), their line-of-sight velocity dispersion should be small, $\sigma_0 \lesssim 3 \text{ km s}^{-1}$.

The second term which enters into σ_{eff} is that arising from the uncertainty of our velocity measurements. This error has two components. The first, which is associated with our centroiding of the [O III] $\lambda 5007$ emission line, is generally small: our velocity measurements typically have errors that are less than $\sim 5 \text{ km s}^{-1}$. This is in agreement with the results of Herrmann & Ciardullo (2009), who used the same telescope and instrument setup to obtain $\lesssim 5 \text{ km s}^{-1}$ precision for faint PNe in distant galaxies.

The other component of the error term, that coming from the absorption line measurements, is more complex. Almost half of our clusters have high-quality ($\sigma_v \lesssim 3 \text{ km s}^{-1}$) velocity measurements, mostly through the MMT + Hectoechelle observations of Strader et al. (2011). As the left panel of Figure 5 shows, there is no systematic difference between our measurements and those of the Hectoechelle. Six clusters have highly discrepant velocities, as they differ from their Strader et al. (2011) values by more than 3 times the internal errors of the measurements. Yet when these objects are removed, the remaining 199 objects have a mean WIYN+Hydra velocity that is just $\Delta V = 0.2 \text{ km s}^{-1}$ greater than that of the Hectoechelle. Since the two sets of observations are on the same system, we can adopt the higher precision Strader et al. (2011) velocities in our analysis.

For most of the remaining clusters, we can use our own velocity measurements, along with their associated measurement errors. As the right panel of Figure 5 illustrates, the dispersion between our independent velocity estimates of clusters observed in more than one Hydra setup is consistent with the expectations of internal measurement error. Moreover, it is possible to obtain a quantitative estimate of our uncertainties by comparing our velocity measurements (and their errors) to those of the Strader et al. (2011) Hectoechelle data using the χ^2 statistic

$$\chi^2 = \sum_i \frac{(v - v_S)_i^2}{(\sigma^2 + \sigma_S^2)_i} \quad (2)$$

where v , σ , v_S , and σ_S represent our velocities and their uncertainties, and those of Strader,

respectively. When the six discrepant systems are removed, the reduced χ^2 for the 199 degrees of freedom is 0.96. This strongly suggests that the internal errors of our velocity determinations are accurate, and can be adopted as the true uncertainties of our measurements.

Finally, as Figure 5 shows, the typical error of our absorption line velocities is between 15 and 20 km s⁻¹. However, a small number of objects have velocity uncertainties that are significantly greater than this. In a few cases, more accurate velocities are available from the literature, and in those cases, we either adopted the previously measured values, or averaged our velocities with the published data. The remaining objects, where our velocity uncertainties were greater than 30 km s⁻¹, were excluded from the analysis. Those clusters for which our velocities disagree with previously measured values by more than four times the internal errors are given in Table 2.

4. The Clusters Hosting Emission

After forming σ_{eff} , we excluded all PN candidates with [O III] $\lambda 5007$ velocities that differed from that of their parent cluster by more than $3\sigma_{\text{eff}}$. We note that this criterion may not remove all the false detections, since young clusters are expected to have kinematics similar to that of the underlying disk. However, for the older systems, this should be a very effective discriminant. Since the rotation-corrected velocity dispersion of M31’s globular cluster system is ~ 130 km s⁻¹ (Lee et al. 2008), the chance of finding a superposed disk source with the same velocity as one of our candidate clusters is extremely low.

Table 3 lists all the cluster candidates surveyed in this program, along with their Washington system photometry obtained with the KPNO 0.9-m telescope (Kim et al. 2007), their radial velocities, the equivalent widths of their [O III] $\lambda 5007$ emission line, their [O III] $\lambda 5007$ to H β emission-line ratio, and an age/type classification. For most of the clusters, this classification comes from the analyses of either Caldwell et al. (2009, 2011) or Peacock et al. (2010), and are based on a variety of measurements, including multi-bandpass photometry, *HST* color-magnitude diagrams, and, in many cases, high signal-to-noise spectra. To infer the ages of the 12 remaining objects without any age classification, we used the clusters with known ages as a training set for our photometry. As Figure 6 illustrates, most of the clusters designated as “young” are quite blue, with $C - T_1 < 1.2$ and $M - T_1 < 0.7$. Conversely, the overwhelming majority of redder clusters are old. Thus for the clusters without a previous age determination, we can use color as a proxy for evolutionary status. We classify any object redder than $C - T_1 = 1.2$ as old; bluer clusters are identified as young. These color-based classifications are designated in Table 3 with a parenthesis.

Table 4 lists those M31 clusters which host possible planetary nebulae, along with the properties of the systems. The signal-to-noise ratios for the [O III] and $H\beta$ emission-line measurements are also tabulated. The first three objects give the candidates associated with stellar systems confirmed as being old; the next five list candidates in the younger clusters. Finally, two of our PN candidates are associated with controversial objects, i.e., cluster candidates which may, in fact, be foreground stars.

To estimate the [O III] $\lambda 5007$ magnitudes of the PNe, we used our knowledge of the 5000 Å continuum brightness of each cluster, as determined by its Washington system M magnitude (central wavelength 5075 Å). By measuring the strength of [O III] $\lambda 5007$ relative to this continuum, i.e., the line’s equivalent width, we could approximate the PN candidate’s 5007 Å monochromatic flux. This flux was then converted to a magnitude via

$$m_{5007} = -13.74 - 2.5 \log F_{5007} \quad (3)$$

and placed on an absolute scale by assuming a distance of 750 kpc (Freedman et al. 2001) and a differential extinction of $E(B - V) = 0.062$ (Schlegel et al. 1998). On this scale, the brightest PNe in M31 attain a luminosity corresponding to $M_{5007} = -4.5$ (Ciardullo et al. 1989; Merrett et al. 2006). This value is fairly resilient against alternative distant estimates to M31 (e.g., 780 kpc; McConnachie et al. 2005).

Of course, estimating brightnesses in this way carries a substantial amount of uncertainty. While the vast majority of M31 globular clusters have half-light radii smaller than the 1.5 radius of our fibers, the tidal radii for these objects extend much farther (Barmby et al. 2007). As a result, the light coming through the fiber may not accurately reflect the total magnitude of the cluster, and astrometric errors in the cluster coordinates and fiber positioning only exacerbate the problem.

Moreover, the position of the emission-line source within the globular cluster is unknown. Even if the fiber is centered on the globular cluster, a point-source planetary nebula may be offset by more than an arcsec. For example, if the four PNe within the Milky Way clusters were placed at the distance of M31, their typical separation from their cluster’s center would be 0.3-0.4", but JaFu 1 in Pal 6 would be offset by a full 1.8". This means that for three out of the four objects, the photometric error due to their position of the PN within the cluster would be negligible (< 1% loss through our 3" fibers), but in 1" seeing, JaFu 1’s luminosity would be underestimated by a factor of ~ 5 . In the absence of high resolution imaging, our spectroscopic [O III] luminosities are the best that can be achieved for these objects, and likely represent lower limits to the true [O III] $\lambda 5007$ brightnesses. Other properties which scale with luminosity, such as the inferred minimum central star mass, would be lower limits as well.

The spectra of our candidate PN-GC associations are shown in Figure 7 and Figure 8. Below we detail their properties.

4.1. Globular Clusters

Jacoby et al. (1997) argued that the single stars of old globular clusters cannot form PNe due to the time scale of their post-AGB evolution: by the time their cores become hot enough for ionization, their ejected gas would have dispersed far into the interstellar medium. Thus, Jacoby et al. (1997) concluded that PN formation inside globular clusters must involve binary stars, either through mass transfer, which increases the core mass to that of a higher mass progenitor, or through a binary interaction which accelerates the speed of post-AGB evolution (Moe & De Marco 2012). More recently, Buell (2012) has suggested an alternative, wherein the single stars of globular clusters evolve high mass cores by being enriched in the helium produced by previous generations of star formation in the cluster. In any scenario, however, central star mass is a critical parameter of the PN system, but one that is very difficult to determine, even for Galactic PNe.

We can, however, place limits on the mass of a PN central star using models of post-AGB evolution. At best, the [O III] $\lambda 5007$ emission of a planetary nebula represents $\sim 10\%$ of the luminosity being emitted from its central star (Dopita et al. 1992; Schönberner et al. 2010). Moreover, for any central star luminosity, there is a minimum core required to generate that energy (Vassiliadis & Wood 1994; Blöcker 1995). If we find that this minimum mass is too high to be produced by the evolution of a single star of an old stellar population, then we will have strong evidence for a previous binary interaction. We apply this approach to our candidate objects.

B115-G177: According to Caldwell et al. (2011), this globular cluster is old and metal-rich, with $[\text{Fe}/\text{H}] \sim +0.1 \pm 0.1$. Yet the system harbors an emission-line source that is bright enough to stand out in an Fe5015 versus Fe5270 plot, and hot enough to have an [O III] $\lambda 5007$ line that is three times the strength of $\text{H}\beta$. To place a lower limit on the luminosity of the exciting source, we can use the fact that no more than $\sim 10\%$ of a central star’s total luminosity is reprocessed into [O III] $\lambda 5007$ (Dopita et al. 1992; Schönberner et al. 2010). Consequently, for a source to be as bright as $M_{5007} \sim -2.2$, its exciting star must be at least $\sim 700 L_{\odot}$ and have a mass of at least $\sim 0.54 M_{\odot}$. Although low-mass cores are capable of generating this amount of luminosity, their evolutionary time scale is too slow to produce a planetary nebula. This is our best candidate for a PN inside an M31 globular cluster and an object formed by binary evolution. It may be coincidental that a rare PN is found in a relatively rare metal-rich, yet old, globular cluster (Woodley et al. 2010), or perhaps the

combination of properties is a clue to PN formation.

BH16: This cluster, classified as old by Strader et al. (2011), possesses the X-ray source J004246.0+411736 (Fan et al. 2005). Our velocity measurement for the system is relatively poor (-248 ± 28 km s⁻¹), due to possible contamination from the underlying galactic bulge, and inconsistent with the -99.9 ± 1.1 km s⁻¹ Hectoechelle measurement obtained by Strader et al. (2011). If we adopt the latter value, then the velocity of the superposed [O III] $\lambda 5007$ emission line differs from that of the cluster by less than 20 km s⁻¹ ($\sim 2.7\sigma_{\text{eff}}$), making an association likely. The emission-line source itself has a high-excitation ($R \sim 4$), but is also relatively faint, implying a central star luminosity that may be as low as $100 L_{\odot}$.

NB89: The Lick indices (González 1993) of this system imply an age of ~ 10 Gyr and a metallicity of $[Z/H] \sim -0.6$ (Barmby et al. 2000; Beasley et al. 2005), so the object is most likely a globular cluster. Its PN candidate is well-measured, but faint, with an estimated [O III] $\lambda 5007$ absolute magnitude that is ~ 4 mag down the luminosity function. The cluster also barely satisfies our selection criteria: [O III] $\lambda 5007$ is just 2.1 times the strength of $H\beta$, and its inclusion in our list is partly due to the large (~ 30 km s⁻¹) uncertainty in our estimate of cluster velocity. If, instead of using our own measurement, we adopt the velocity of -332 ± 6 km s⁻¹ observed by Barmby et al. (2000), then the emission-line’s velocity of -384 ± 5 km s⁻¹ is no longer consistent with it being part of the cluster. Caldwell (priv. comm.) reports that forbidden emission from [O II] and [S II] are strong, further suggesting that the emission-lines are interstellar in nature.

4.2. Candidate Globular Clusters

SK044A: Caldwell et al. (2009) classify this object as an M31 cluster (of indeterminate age) based on its spectrum and its profile on archival *HST* frames. In contrast, Peacock et al. (2010) call the object a star, citing their analysis of UKIRT and SDSS data. We also have difficulty classifying the object: although the cluster’s neutral color places it 0.062 ± 0.056 mag blueward of our “young” versus “old” dividing line, its measured radial velocity differs from that of M31’s underlying disk by ~ 100 km s⁻¹ (Chemin et al. 2009). Further complicating the interpretation is our relatively poor determination for the cluster velocity (-518 ± 39 km s⁻¹): even when combined with the -491 ± 46 km s⁻¹ measurement of Kim et al. (2007), the resultant ± 29 km s⁻¹ uncertainty still dominates the error budget. Nevertheless, the system is interesting, since its emission line velocity is inconsistent with a warm disk origin, and, with an [O III] $\lambda 5007$ to $H\beta$ ratio of $\gtrsim 12$, it has the highest emission-line excitation in our sample. The [O III] $\lambda 5007$ line is faint, so that if the emission is powered by a PN, its central star could be fainter than $\sim 150 L_{\odot}$. Unfortunately, without better

velocity information, we cannot say for certain whether the observed 48 km s^{-1} difference between the cluster’s emission lines and absorption features is indicative of an association or a chance superposition. Caldwell (priv. comm.) notes that [S II] is weak in his spectrum, providing further support for the idea that the emission line is produced in a PN rather than the warm interstellar medium.

SK051A: This is our faintest PN candidate, and another object for which we have a relatively large (22 km s^{-1}) measurement error. Nevertheless, our derived cluster velocity is in excellent agreement with that found by Kim et al. (2007), and the source does possess high-excitation ($R > 5$) [O III] emission at a velocity consistent with both estimates. The system has the colors of an old cluster, but without better data, we cannot confirm its association with the emission line. Peacock et al. (2010) classify the object as a foreground star based on its appearance on images from UKIRT and SDSS, and Caldwell (priv. comm.) notes that the object is not resolved on *HST* frames. Thus, it is possible that the observed continuum is from a point source contaminant, rather than a compact cluster.

4.3. Young Clusters

B458-D049: The cluster just barely satisfies our criterion, as the velocity of the [O III] $\lambda 5007$ emission-line differs from that of the cluster by 18 km s^{-1} , or $2.9 \sigma_{\text{eff}}$. It is a young system, as evidenced by the poor results of our template subtraction about the $H\beta$ absorption line, and Caldwell et al. (2009) estimate its age at 0.5 Gyr. If the [O III] emission does come from a planetary, then the physics of single-star stellar evolution implies that the PN is a high core-mass object. Specifically, the relationship between age and turnoff mass (Iben & Laughlin 1989), coupled with the initial mass-final mass relation (Kalirai et al. 2008) yields $M_{\text{core}} \sim 0.66 M_{\odot}$. If the emission does come from a cluster PN, then the object either evolved from a single massive (young) star and is now well-past its peak [O III] $\lambda 5007$ brightness of $\sim 8000 L_{\odot}$, or it was created through a binary pathway and is likely the result of common envelope evolution. One can sometimes distinguish between these two possibilities in the Galaxy where morphology and abundance anomalies provide some discrimination (Miszalski et al. 2013). At the distance of M31, luminosity is the primary indicator; if an object is very bright, then it likely derives from a single massive star.

M040: Caldwell et al. (2011) re-classified this object as young, though they did not estimate an age. [O III] $\lambda 5007$ is well-measured, [O III] $\lambda 4959$ is weak, and $H\beta$ is virtually undetectable. The velocity agreement between the set of emission lines and that of the underlying cluster continuum is not particularly good, between 13 and 28 km s^{-1} , depending on whether we adopt our velocity or that of Caldwell et al. (2011). Given the $\sim 30 \text{ km s}^{-1}$

uncertainties of both measurements, an association remains a possibility.

C009-LGS04131: Our velocity for this faint system is poor ($-483 \pm 51 \text{ km s}^{-1}$) but it is in excellent agreement with the value of $-495 \pm 32 \text{ km s}^{-1}$ measured by Caldwell et al. (2009) and with the velocity of its [O III] $\lambda 5007$ emission line ($-484 \pm 5 \text{ km s}^{-1}$). The cluster itself is young, with an age of $\sim 0.3 \text{ Gyr}$ (Caldwell et al. 2009) and a turnoff mass of $\sim 3.1 M_{\odot}$ (Iben & Laughlin 1989). Although [O III] $\lambda 5007$ is rather faint, ($M_{5007} \sim +1.7$), it is well-measured, and whatever is causing the emission has a very high excitation, $R > 6$. If the exciting source is a planetary, then, based on the turnoff mass, it is either a $\sim 0.73 M_{\odot}$ core mass object which has faded substantially since its peak luminosity, or an object that was formed through a binary interaction.

SK018A: We observed this young cluster twice, with consistent results ($\Delta v = 6.5 \text{ km s}^{-1}$). Caldwell et al. (2009) estimate the age of the cluster to be $\sim 0.8 \text{ Gyr}$, which implies a turnoff mass of $\sim 2.1 M_{\odot}$ (Iben & Laughlin 1989) and a PN core mass of $\sim 0.62 M_{\odot}$ (Kalirai et al. 2008). Like C009-LGS04131, the object is more than $\sim 6 \text{ mag}$ down the [O III] $\lambda 5007$ PNLF. There is no evidence of $H\beta$, which implies $R > 4$.

DAO47: Our velocity, when combined with two other determinations in the literature (Perrett et al. 2002; Caldwell et al. 2009), yields a value that is within 9 km s^{-1} of that measured for the [O III] line. The spectrum is relatively noisy, and even after template-subtraction, residual stellar $H\beta$ absorption is still visible. Nevertheless, [O III] $\lambda 5007$ is reasonably well-detected, and the narrow $H\beta$ emission line is completely absent. Caldwell et al. (2009) estimate the age of the system to be $\sim 0.5 \text{ Gyr}$, which, in terms of turnoff mass, is $\sim 2.5 M_{\odot}$ (Iben & Laughlin 1989). The initial mass-final mass relation then implies $M_{\text{core}} \sim 0.66 M_{\odot}$.

5. Discussion

5.1. Expected and Observed Numbers of PN Candidates

In their survey of 130 Milky Way globular clusters, Jacoby et al. (1997) identified four planetary nebulae. Since our M31 survey targeted ~ 270 old clusters, a simple scaling of numbers suggests that we should have found ~ 8 PNe in our survey. However, only two of the Milky Way objects (Ps 1 in M15 and JaFu 1 in Pal 6) would have been definitively detected by our observations. At the distance of M31, JaFu 2, which is 7.3 mag down the PNLF, would be at, or just below, the threshold for detection, and GJJC-1 in M22 (which may not be a true PN) would be well past our detection limit. Consequently, we might expect to see ~ 4 objects; our list of systems with PN candidates contains 3 confirmed globular clusters,

and two other sources which may be old systems.

It is unlikely that all of these candidates are true PNe, but the data are marginally consistent with the results of the Galactic surveys. Of the 5 candidates, 1 appears to be an excellent PN identification associated with an old cluster. If the other 4 candidates are ultimately rejected, then the number of PNe in M31 globular clusters found in this study is 4 times lower than expected. This can be explained, in part, as a consequence of the observational challenges of the project.

Similarly, our data are consistent with the results of the Peacock et al. (2012) survey of the Virgo giant elliptical NGC 4472. Their observations of 174 luminous globular clusters covered $\sim 2 \times 10^8 L_\odot$ of bolometric light, and extended ~ 2.5 mag down the PN luminosity function. Our observations surveyed ~ 2.5 times less light, but extended ~ 3.5 mag further down the PN luminosity function. If we assume that the PNLF of globular clusters is similar to that of the field stars of old populations, i.e.,

$$N(M) \propto e^{0.307M} \{1 - e^{3(M^* - M)}\} \quad (4)$$

then the NGC 4472 observations imply that we should have seen $\lesssim 2$ PN in our survey. This, again, is consistent with our data.

Conversely, the number of PN candidates found in young clusters is far more than anticipated. The total luminosity of all the young clusters included in our survey list is rather small, $M_V \sim -9.6$, and only $M_V \sim -8.6$ was surveyed with good velocity precision. Because the young clusters are members of the disk population, their velocities are far more likely to match the velocities of potential interlopers (e.g., HII regions, SNRs, disk emission) that are also in the disk, than would the old clusters. We therefore must exercise additional caution when evaluating these candidate PNe.

If we assume a bolometric correction of -0.85 (Buzzoni et al. 2006), this implies that our survey of young clusters sampled $\sim 5 \times 10^5 L_\odot$ of light. From the theory of stellar energy generation, the bolometric luminosity stellar evolutionary flux for systems with ages between ~ 0.1 and ~ 1 Gyr is $\sim 1 \times 10^{-11}$ stars $\text{yr}^{-1} L_\odot^{-1}$ (Renzini & Buzzoni 1986). Thus, we might expect these populations to produce one PN every $\sim 200,000$ years. Even if these PNe remained visible for 50,000 yr, that is still not enough time to build up a detectable population. It is therefore likely that the larger velocity errors associated with these fainter clusters, and the kinematic similarity of the clusters and the field exacerbate our ability to discriminate PN candidates from superposed disk emission.

5.2. Are Binary Stars Important

Ciardullo et al. (2005) have argued that blue stragglers are responsible for most, if not all, of the bright PNe found in elliptical galaxies. Not only do these objects possess the main-sequence masses needed to build high-mass post-AGB cores, but their evolutionary timescale, relative to that of PN ($\sim 10^6$), is roughly the same as the relative numbers of the two objects. Since the creation of blue stragglers in globular clusters may, in some way, be related to the rate of stellar encounters, Γ (i.e., Davies et al. 2004; Leigh et al. 2011), then it is at least possible that the probability of finding a PN would also be proportional to this factor. From Verbunt & Hut (1987), this means that

$$N(PN) \propto \Gamma \propto \frac{\rho_0^2 r_c^3}{\sigma} \quad (5)$$

where ρ_0 is the cluster’s central luminosity density, r_c is the core radius, and σ is the stellar velocity dispersion. The structural parameters of Milky Way clusters (Harris 1996, 2010) do seem to support this idea, as two of the systems which host PNe have extremely high encounter rates (NGC 6441 has the second highest rate of all Galactic GCs, and M15’s rate ranks as seventh), and three of the four rank in the top half of clusters. Moreover, this result is not simply due to the clusters having more stars: if one calculates the mass-specific encounter rates of the Milky Way clusters, then again, three of the four clusters hosting PNe appear in the top half of the list. The statistics of only four objects are poor, but the numbers do suggest a connection between stellar encounters and PN formation.

Unfortunately, our emission-line survey of M31’s globular cluster system does not yet allow us to increase the statistics significantly. Although over 250 of M31’s globular clusters have structural measurements (Barmby et al. 2007; Peacock et al. 2010), only one of the old clusters listed in Table 4 are included in that number. Interestingly, if we assume that the clusters are in virial equilibrium (so that we can approximate the encounter rate using $\Gamma \propto \rho_0^{1.5} r_c^2$), then the cluster in question (B115-G177, which contains our best PN candidate) has a value of Γ that ranks in the top $\sim 25\%$ of M31 systems. This again is suggestive, but it cannot be considered definitive until the other systems listed in Table 4 are surveyed.

Alternatively, we can attempt to explore the frequency of stellar encounters using X-ray emission as a proxy for encounter rate. Pooley et al. (2003) have shown that in Galactic globular clusters, there is an excellent correlation between Γ and the number of low-mass X-ray binaries (LMXBs). If each LMXB had the same luminosity, we could test the PN binary-formation hypothesis by searching for a correlation between PN presence and X-ray brightness. Jacoby et al. (1997) did this experiment in the Milky Way, where each individual X-ray source can be identified. This led the authors to suggest that binaries were responsible for the cluster planetary nebulae.

In M31, one cannot resolve the individual X-ray sources within each cluster, and counting the total X-ray emission from a GC is not the same as measuring its total LMXB population. In fact, the large range of luminosities possible for LMXBs makes any connection between X-ray luminosity and binary population tenuous at best. In our survey, $\sim 15\%$ of the globular clusters have X-ray sources, but only one appears in Table 4 (Stiele et al. 2011). Consequently, X-ray emission in M31 clusters does not appear to present any evidence for the PN binary formation hypothesis.

5.3. The Luminosities of the Candidates

Figure 9 displays the [O III] $\lambda 5007$ magnitudes of planetary nebulae associated with Milky Way and M31 clusters. From the figure, it is clear that most of the clusters found in our spectroscopic survey are far fainter than those discovered via narrow-band or counter-dispersed imaging. This is simply a consequence of the technique; slit spectroscopy reduces the sky background enormously, allowing us to probe a region of M31’s PN luminosity function that is undetectable by other methods.

The more salient feature of the diagram is the distribution of relative PN luminosities. The systems of globular clusters in the Milky Way and M31 each contain a lone bright PN candidate; the remaining objects are extremely faint, in a regime where the luminosity function of LMC PNe is increasing exponentially (Reid & Parker 2010). This is expected if most faint PNe have slowly evolving central stars embedded in freely expanding nebulae (Henize & Westerlund 1963). In globular clusters, however, we might expect the PNLF to be distorted, as the absence of intermediate mass stars might result in a deficit of intermediate luminosity PNe. Thus far, however, there is no evidence for this effect: according to a Kolmogorov-Smirnov test, the combined luminosity function of PNe in Milky Way and M31 globular clusters is fully consistent with the curve displayed in Figure 9. Of course, the numbers involved are small, but to date, there is no reason to reject the hypothesis that the PNe of globular clusters obey the simple law proposed by Ciardullo et al. (1989).

5.4. The Observational Challenge

For Galactic clusters, searching for PNe is relatively straightforward. As demonstrated by Jacoby et al. (1997), one can use the classic on-band/off-band technique to detect [O III] $\lambda 5007$ over almost the entire planetary nebula luminosity function. Moreover, one can resolve both the cluster stars (except near the cluster center) and, importantly, the nebula.

These two factors enable easy detection of emission-line objects having the morphological characteristics of a PN, even at very low surface brightnesses. Furthermore, relative to an extragalactic survey, cluster classifications are far more reliable, as are the velocity measurements for both the PN and the cluster.

In contrast, attempts to identify PNe in other galaxies are faced with a host of complications. Among these are:

Mimics: Objects other than PNe (e.g., H II regions, SNRs, and diffuse emission) can have similar spectral signatures over the limited wavelength range of the WIYN Bench Spectrograph and its 740 lines mm VPH grating. This problem is partially technical, as many modern spectrographs offer more complete spectral coverage at comparable resolution, allowing better discrimination against potential mimics. Yet even in the Milky Way, PN classifications can be controversial (e.g., Viironen et al. 2009; Frew & Parker 2010) and PN candidates are constantly being re-evaluated. The limited information available on extragalactic objects only exacerbates this problem.

Spectral resolution and sensitivity: These instrumental parameters are probably the most critical factors for successfully and definitively finding PNe in extragalactic globular clusters. As described above, our ability to define the velocity (and the velocity dispersion) of the underlying star cluster severely limited our ability to exclude chance superpositions. We were fortunate that the literature provided an excellent source of velocities for many of our objects. For searches beyond M31, $\lesssim 3 \text{ km s}^{-1}$ velocity measurements will not always be available. Similarly, sensitivity becomes increasingly important at larger distances, both for determining cluster velocities and for probing the faint end of PNLf. The study in NGC 4472 (Peacock et al. 2012) only reached 2.5 mag down the PNLf; had we not gone far beyond this limit in M31, we likely would not have identified any PN candidates. Finally, resolution is also a helpful factor in this type of survey, both for the detection of PN emission, and for eliminating mimics such as SNRs and nova shells, which will have broad emission lines. Again, this is a technical issue where large telescopes can dramatically advance studies like this one.

Spectral aperture (slit width, fiber size): Our fiber diameter was limited to $3''$, which is a reasonable match to the half-light radius of most M31 clusters. Still, these fibers do not sample all of the cluster light, and outlying PN could be overlooked, either because they fall entirely outside the fiber, or near the fiber limits, where flux is lost due to the effects of seeing. One could, of course, choose to use a large fiber or slit size for the observation (though at WIYN, the largest fiber size is $3''$), but this would reduce the signal-to-noise of the measurement by admitting more sky and galactic background. This problem is ameliorated when going to more distant galaxies, though again at the cost of a higher galactic background

and a loss of sensitivity due to the greater distance.

Multiple objects along the line of sight: When observing a distant galaxy, there is a finite probability that two unrelated objects will fall within the same spectroscopic aperture. This problem becomes worse as the distance increases, as a given fixed aperture represents a broader spatial swath of the galaxy. To compensate for this effect, one needs better velocity measurements so that unrelated objects can be discriminated.

In the future, searches for PNe in extragalactic globular clusters should be more productive as many of these challenges can be overcome with technological advancements. For example, the M31 problem becomes relatively easy with the high signal-to-noise spectra produced by an extremely large (25-40 m class) telescope (ELT) equipped with a multiobject, dual-channel, medium-resolution spectrograph. Similarly, adaptive optics on ELTs (or narrow-band filters on the *Hubble Space Telescope* could be used to resolve the cluster into stars, allowing the PN candidate to be imaged directly. This technique would not work as well for systems beyond a few Mpc, but could produce a complete census of cluster PN in the nearby universe.

6. Conclusions

We have demonstrated that it is possible to identify PN candidates in distant globular clusters using spectroscopy around the [O III] $\lambda 5007$ emission line. The principal difficulty in this approach lies in confirming that the candidates are, indeed, associated with the cluster. This requires precise radial velocity measurements, both for the emission line, and the underlying stellar continuum. The better the velocity resolution of the survey, the easier it is to separate embedded PNe from chance superpositions, and to distinguish a cluster-bound PN from other unrelated emission-line sources along the line of sight, such as H II regions, SNRs, and diffuse emission.

Of the 270 M31 globular cluster candidates observed with sufficient velocity precision, five show evidence for a candidate planetary nebula. Given the luminosity limits of the survey, the uncertainties in the velocity measurements, and the potential for confusion with other emission-line sources, this result is marginally consistent with the rate of PNe found in Milky Way clusters, i.e., 3 or 4 in 130 clusters, and the upper limit found in a survey of globular clusters around NGC 4472. This rate argues that less than one-quarter of the stars in old clusters form PNe (Jacoby et al. 1997). These numbers are also marginally consistent with the binary hypothesis for PN formation, which is about four times higher than the single star production rate in old clusters (Moe & De Marco 2006).

At this time we cannot say how many cluster-associated PNe are likely to have been formed from binary interactions. Only one M31 PN candidate is embedded in a cluster whose structural parameters are known, but based on that cluster’s properties, and on the properties of the Milky Way’s PN clusters, it appears that the binary evolution scenario is a viable hypothesis to explain all globular cluster PNe. High resolution imaging would help confirm the existence of our PN candidates, and provide structural information on the host clusters.

In addition, we identified five PN candidates among the young clusters in our sample, a number that is much higher than that expected from the luminosity specific stellar death rate. These are likely superpositions; most of the young systems surveyed have large velocity uncertainties, and the similarity between their kinematics and that of the underlying disk make it difficult to identify superposed objects.

Finally, we emphasize that the M31 objects listed in Table 4 are PN candidates only. *Hubble Space Telescope* narrow-band images are needed to confirm their existence, especially for those objects within young clusters. However, once confirmed, these targets represent a new source of material for understanding the physics of PN formation, and the chemistry of their parent clusters.

Acknowledgments

We wish to thank Laura Fullton for early discussions about this project, and Nelson Caldwell for helpful insights and providing access to his M31 cluster web page (http://www.cfa.harvard.edu/oir/eg/m31clusters/M31_Hectospec.html). MGL is supported in part by the Mid-career Researcher Program through an NRF grant funded by the MEST (No. 2010-0013875). EK was supported by the NOAO/KPNO Research Experiences for Undergraduates (REU) Program, which is funded by the National Science Foundation (NSF) Research Experience for Undergraduates Program and the Department of Defense ASSURE program through Scientific Program Order No. 13 (AST-0754223) of the Cooperative Agreement No. AST-0132798 between the Association of Universities for Research in Astronomy (AURA) and the NSF.

REFERENCES

- Abell, G.O., & Goldreich, P. 1966, *PASP*, 78, 232
- Barmby, P., Huchra, J.P., Brodie, J.P., Forbes, D.A., Schroder, L.L., & Grillmair, C.J. 2000, *AJ*, 119, 727
- Barmby, P., McLaughlin, D.E., Harris, W.E., Harris, G.L.H., & Forbes, D.A. 2007, *AJ*, 133, 2764
- Barmby, P., Perina, S., Bellazzini, M., Cohen, J.G., Hodge, P.W., Huchra, J.P., Kissler-Patig, M., Puzia, T.H., & Strader, J. 2009, *AJ*, 138, 1667
- Beasley, M.A., Brodie, J.P., Strader, J., Forbes, D.A., Proctor, R.N., Barmby, P., & Huchra, J.P. 2005, *AJ*, 129, 1412
- Bergond, G., Zepf, S.E., Romanowsky, A.J., Sharples, R.M., & Rhode, K.L. 2006, *A&A*, 448, 155
- Bershady, M., et al., 2008, *SPIE*, 7014, 15
- Bessell, M.S. 2001, *PASP*, 113, 66
- Bianchi, L., Bohlin, R., Catanzaro, G., Ford, H., & Manchado, A. 2001, *AJ*, 122, 1538
- Blair, W.P., Kirshner, R.P., & Chevalier, R.A. 1982, *ApJ*, 254, 50
- Blöcker, T. 1995, *A&A*, 299, 755
- Buell, J.F., 2012, *MNRAS*, 419, 2867
- Buzzoni, A., Arnaboldi, M., & Corradi, R.L.M. 2006, *MNRAS*, 368, 877
- Caldwell, N., Harding, P., Morrison, H., Rose, J.A., Schiavon, R., & Kriessler, J. 2009, *AJ*, 137, 94
- Caldwell, N., Schiavon, R., Morrison, H., Rose, J.A., & Harding, P. 2011, *AJ*, 141, 61
- Caloi, V. 1989, *A&A*, 221, 27
- Chemin, L., Carignan, C., & Foster, T. 2009, *ApJ*, 705, 1395
- Chomiuk, L., Strader, J., & Brodie, J.P. 2008, *AJ*, 136, 234
- Ciardullo, R., Feldmeier, J.J., Jacoby, G.H., Kuzio de Naray, R., Laychak, M.B., & Durrell, P.R. 2002, *ApJ*, 577, 31

- Ciardullo, R., Rubin, V., Ford, W.K., Jacoby, G.H., & Ford, H.C., 1988, *AJ*, 95, 438
- Ciardullo, R., Jacoby, G.H., & Ford, H.C. 1989, *ApJ*, 344, 715
- Ciardullo, R., Sigurdsson, S., Feldmeier, J.J., & Jacoby, G.H. 2005, *ApJ*, 629, 499
- Davies, M.B., Piotto, G., & de Angeli, F. 2004, *MNRAS*, 349, 129
- De Marco, O. 2009, *PASP*, 121, 316
- De Marco, O. 2011, in *Asymmetrical Planetary Nebulae V*, ed. A. Zijlstra, I. McDonald & E. Lagadec, Jodrell Bank Centre for Astrophysics, 251
- De Marco, O., Jacoby, G.H., Davies, J., Bond, H.E., & Harrington, P. 2011, *BAAS*, 43, 152
- De Marco, O., Passy, J-C., Frew, D.J., Moe, M., & Jacoby, G.H., 2012, *MNRAS*, in press
- Djorgovski, S.G., Gal, R.R., McCarthy, J.K., Cohen, J.G., de Carvalho, R.R., Meylan, G., Bendinelli, O., & Parmeggiani, G. 1997, *ApJ*, 474, L19
- Dopita, M.A. Jacoby, G.H., & Vassiliadis, E. 1992, *ApJ*, 389, 27
- Fan, Z., Ma, J., Zhou, X., Chen, J., Jiang, Z., & Wu, Z. 2005, *PASP*, 117, 1236
- Frankowski, A., & Soker, N. 2009, *ApJ*, 703, L95
- Freedman, W.L., Madore, B.F., Gibson, B.K., Ferrarese, L., Kelson, D.D., Sakai, S., Mould, J.R., Kennicutt, R.C. Jr., Ford, H.C., Graham, J.A., Huchra, J.P., Hughes, S.M.G., Illingworth, G.D., Macri, L.M., & Stetson, P.B. 2001, *ApJ*, 553, 47
- Frew, D.J., & Parker, Q.A. 2010, *PASA*, 27, 129
- Galarza, V.C., Walterbos, R.A.M., & Braun, R. 1999, *AJ*, 118, 2775
- Galleti, S., Federici, L., Bellazzini, M., Fusi Pecci, F., & Macrina, S. 2004, *A&A*, 416, 917
- Galleti, S., Federici, L., Bellazzini, M., Buzzoni, A., & Fusi Pecci, F. 2006, *A&A*, 456, 985
- Galleti, S., Bellazzini, M., Federici, L., Buzzoni, A., & Fusi Pecci, F. 2007, *A&A*, 471, 127
- Gillett, F.C., Neugebauer, G., Emerson, J.P., & Rice, W.L. 1986, *ApJ*, 300, 722
- González, J.J., 1993, PhD. thesis, Univ. California, Santa Cruz
- Greenawalt, B., Walterbos, R.A.M., & Braun, R. 1997, *ApJ*, 483, 666

- Harrington, J.P., & Platoglou, G. 1993, *ApJ*, 411, L103
- Harris, W.E. 1996, *AJ*, 112, 1487
- Harris, W.E. 2010, arXiv:1012.3224
- Henize, K.G., & Westerlund, B.E. 1963, *ApJ*, 137, 747
- Herrmann, K.A., & Ciardullo, R. 2009, *ApJ*, 703, 894
- Howard, J.W., Henry, R.B.C., & McCartney S. 1997, *MNRAS*, 284, 465
- Iben, I., Jr., & Laughlin, G. 1989, *ApJ*, 341, 312
- Jacoby, G.H., De Marco, O., Lotarevich, I., Lahm, L., Bond, H.E., & Harrington, P. 2013, in preparation
- Jacoby, G.H., Morse, J.A., Fullton, L.K., Kwitter, K.B., & Henry, R.B.C. 1997, *AJ*, 114, 2611
- Jacoby, G.H., Hunter, D.A., & Christian, C.A. 1984, *ApJS*, 56, 257
- Kalirai, J.S., Hansen, B.M.S., Kelson, D.D., Reitzel, D.B., Rich, R.M., & Richer, H.B. 2008, *ApJ*, 676, 594
- Kent, S.M. 1987, *AJ*, 93, 816
- Kim, S.C., Lee, M.G., Geisler, D., Sarajedini, A., Park, H.S., Hwang, H.S., Harris, W.E., Seguel, J.C., & von Hippel, T. 2007, *AJ*, 134, 706
- Larsen, S.S. 2008, *A&A*, 477, L17
- Lee, M.G., Hwang, H.S., Kim, S.C., Park, H.S., Geisler, D., Sarajedini, A., & Harris, W.E. 2008, *ApJ*, 674, 886
- Leigh, N., Sills, A., & Knigge, C. 2011, *MNRAS*, 416, 1410
- Majaess, D.J., Turner, D.G., & Lane, D.J. 2007, *PASP*, 119, 1349
- Magnier, E.A., Prins, S., van Paradijs, J., Lewin, W.H.G., Supper, R., Hasinger, G., Pietsch, W., & Truemper, J. 1995, *A&A*, 114, 215
- Massey, P., McNeill, R.T., Olsen, K.A.G., Hodge, P.W., Blaha, C., Jacoby, G.H., Smith, R.C., & Strong, S.B. 2007, *AJ*, 134, 2474

- McConnachie, A.W., Irwin, M.J., Ferguson, A.M.N., Ibata, R.A., Lewis, G.F., & Tanvir, N. 2005, *MNRAS*, 356, 979
- Merrett, H.R., Merrifield, M.R., Douglas, N.G., Kuijken, K., Romanowsky, A.J., Napolitano, N.R., Arnaboldi, M., Capaccioli, M., Freeman, K.C., Gerhard, O., Coccato, L., Carter, D., Evans, N.W., Wilkinson, M.I., Halliday, C., & Bridges, T.J. 2006, *MNRAS*, 369, 120
- Minniti, D., & Rejkuba, M. 2002, *ApJ*, 575, L59
- Miszalski, B., Napiwotzki, R., Cioni, M.-R.L., Groenewegen, M.A.T., Oliveira, J.M., & Udalski, A. 2011, *A&A*, 531, A157
- Miszalski, B., Boffin, H.M.J., & Corradi, R.L.M., 2013, *MNRAS*, 428, L39
- Moe, M., & De Marco, O. 2006, *ApJ*, 650, 916
- Moe, M., & De Marco, O. 2012, in *I.A.U. Symp. 283, Planetary Nebulae: An Eye to the Future*, ed. A. Manchado, L. Stanghellini, & D. Schönberner (Cambridge), 340
- Parker, Q.A., Frew, D.J., Miszalski, B., Kovacevic, A.V., Frinchaboy, P.M., Dobbie, P.D., & Köppen, J., 2011, *MNRAS*, 413, 1835
- Peacock, M.B., Maccarone, T.J., Knigge, C., Kundu, A., Waters, C.Z., Zepf, S.E., & Zurek, D.R. 2010, *MNRAS*, 402, 803
- Peacock, M.B., Zepf, S.E., & Maccarone, T.J. 2012, *ApJ*, 752, 90
- Pease, F.G. 1928, *PASP*, 40, 342
- Perrett, K.M., Bridges, T.J., Hanes, D.A., Irwin, M.J., Brodie, J.P., Carter, D., Huchra, J.P., & Watson, F.G. 2002, *AJ*, 123, 2490
- Pietsch, W., Fliri, J., Freyberg, M.J., Greiner, J., Haberl, F., Riffeser, A., & Sala, G. 2005, *A&A*, 442, 879
- Pooley, D., Lewin, W.H.G., Anderson, S.F., Baumgardt, H., Filippenko, A.V., Gaensler, B.M., Homer, L., Hut, P., Kaspi, V.M., Makino, J., Margon, B., McMillan, S., Portegies Zwart, S., van der Klis, M., & Verbunt, F. 2003, *ApJ*, 591, L131
- Reid, W.A., & Parker, Q.A. 2010, *MNRAS*, 405, 1349
- Renzini, A., & Buzzoni, A. 1986, in *Spectral Evolution of Galaxies*, ed. C. Chiosi & A. Renzini (Dordrecht: Reidel), 195

- Remillard, R.A., Rappaport, S., & Macri, L.M. 1995, *ApJ*, 439, 646
- Schlegel, D.J., Finkbeiner, D.P., & Davis, M. 1998, *ApJ*, 500, 525
- Schönberner, D., Jacob, R., Sandin, C., & Steffen, M. 2010, *A&A*, 523, A86
- Shklovskii, I.S. 1956, *Astr. Zh.*, 33, 315
- Soker, N. 1997, *ApJS*, 112, 487
- Soker, N. 2006, *ApJ*, 640, 966
- Strader, J., Smith, G.H., Larsen, S., Brodie, J.P., & Huchra, J.P. 2009, *AJ*, 138, 547
- Strader, J., Caldwell, N., & Seth, A.C. 2011, *AJ*, 142, 8
- Stiele, H., Pietsch, W., Haberl, F., Hatzidimitriou, D., Barnard, R., Williams, B.F., Kong, A.K.H., & Kolb, U. 2011, *A&A*, 534, 55
- Vassiliadis, E., & Wood, P.R. 1994, *ApJS*, 92, 125
- Verbunt, F., & Hut, P. 1987, in *I.A.U. Symp. 125, The Origin and Evolution of Neutron Stars*, ed. D.J. Helfand & J.-H. Huang (Dordrecht: Reidel), 187
- Viironen, K., Greimel, R., Corradi, R.L.M., Mampaso, A., Rodríguez, M., Sabin, L., Delgado-Inglada, G., Drew, J.E., Giammanco, C., González-Solares, E.A., Irwin, M.J., Miszalski, B., Parker, Q.A., Rodríguez-Flores, E.R., & Zijlstra, A. 2009, *A&A*, 504, 291
- Woodley, K.A., Harris, W.E., Puzia, T.H., Matías, G., Harris, G.L., & Geisler, D., 2010, *ApJ*, 708, 1335

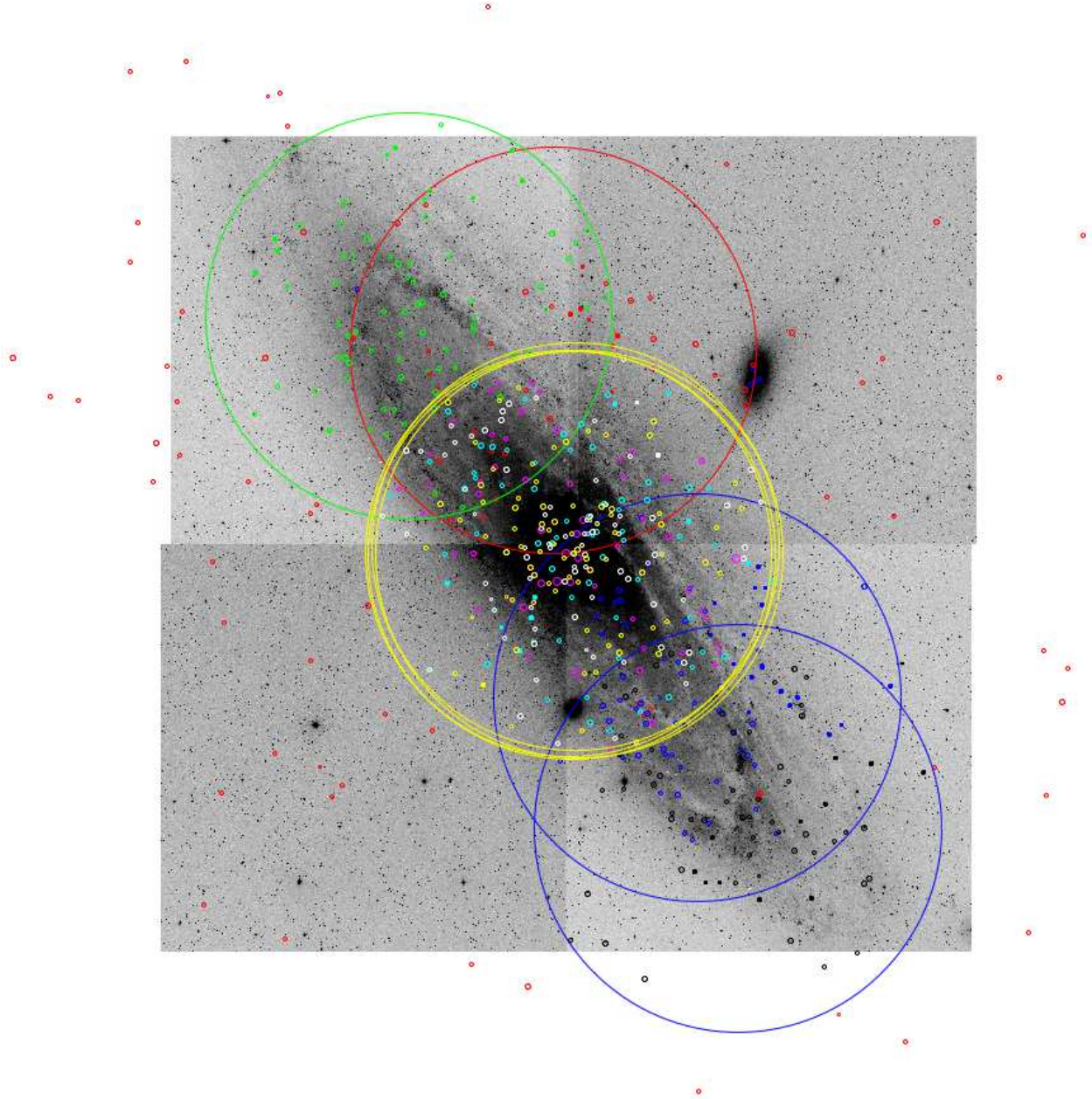


Fig. 1.— The locations of our WIYN+Hydra fields and the targeted M31 clusters, superposed on a mosaic of [O III] images from Massey et al. (2007). North is up, and east is to the left. Each 1° colored circle represents a different Hydra setup.

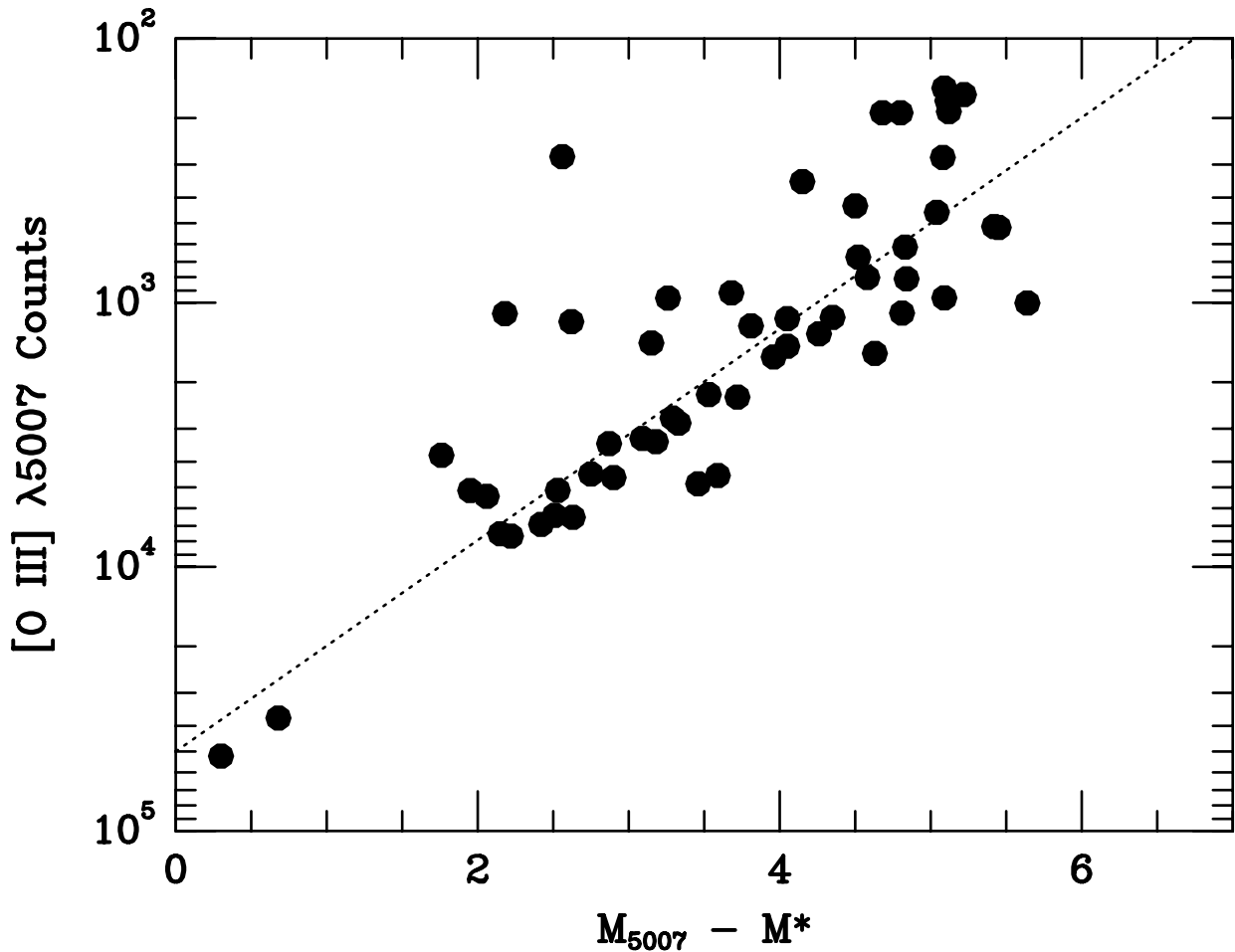


Fig. 2.— A comparison of the absolute [O III] magnitudes of M31 PNe measured by Merrett et al. (2006) to the number of $\lambda 5007$ counts recorded in our spectra. The scatter is due to imperfect astrometry and fiber positioning errors, and the effect of clouds on one of the Hydra setups. The dotted line shows the one-to-one relation. The figure illustrates that we should be able to detect PNe that are more than ~ 6 mag down the luminosity function. For reference, $M^* = -4.5$, which in M31 is equivalent to a monochromatic flux of 2.9×10^{-14} ergs cm^{-2} s^{-1} .

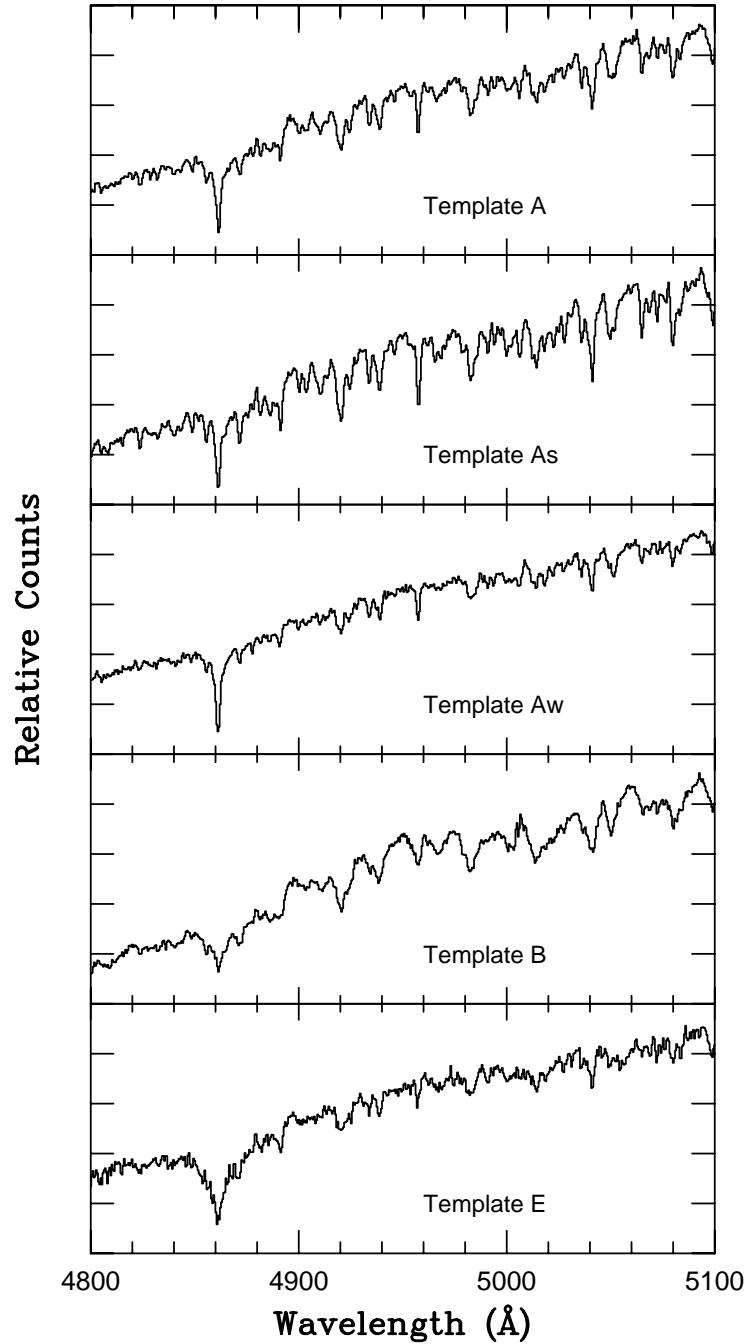


Fig. 3.— Spectra of the five template clusters used to suppress the stellar continuum and enhance the visibility of emission lines. The strongest absorption in this part of the spectrum comes from H β ; most of the others lines are due to iron. The differences between spectra represent variations in cluster’s age and metallicity.

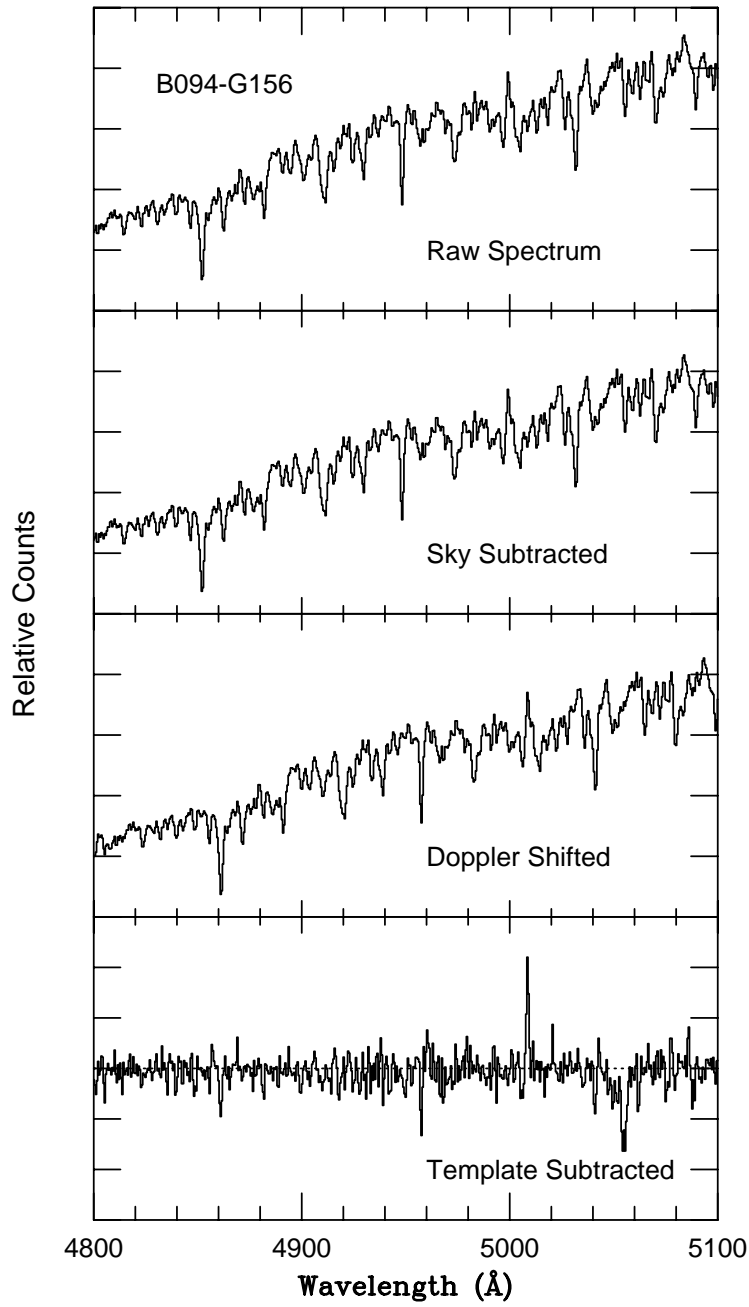


Fig. 4.— The spectra of an M31 globular cluster between 4800 Å and 5100 Å, showing our raw data, along with the data after sky subtraction, Doppler shifting, and template subtraction. Note that after template subtraction, the [O III] λ 5007 emission line is easily seen. This is a well-detected and well-measured emission-line source containing ~ 1000 counts in [O III] λ 5007.

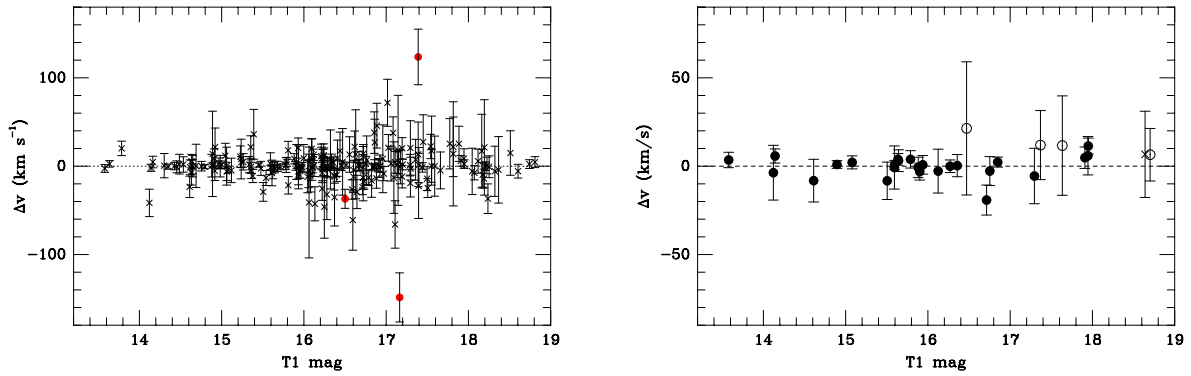


Fig. 5.— Two estimates of the precision of our globular cluster velocities. The left panel compares our data to those of the high-precision measurements of Strader et al. (2011). The solid red points denote objects that differ from zero by more than three times the internal precision of the measurements; three additional systems have velocity discrepancies that fall well off the plot. The right panel shows the velocity differences for clusters observed in more than one Hydra setup. The scatter in these data is 7.6 km s^{-1} . Solid points display old (globular) clusters; open circles show younger systems.

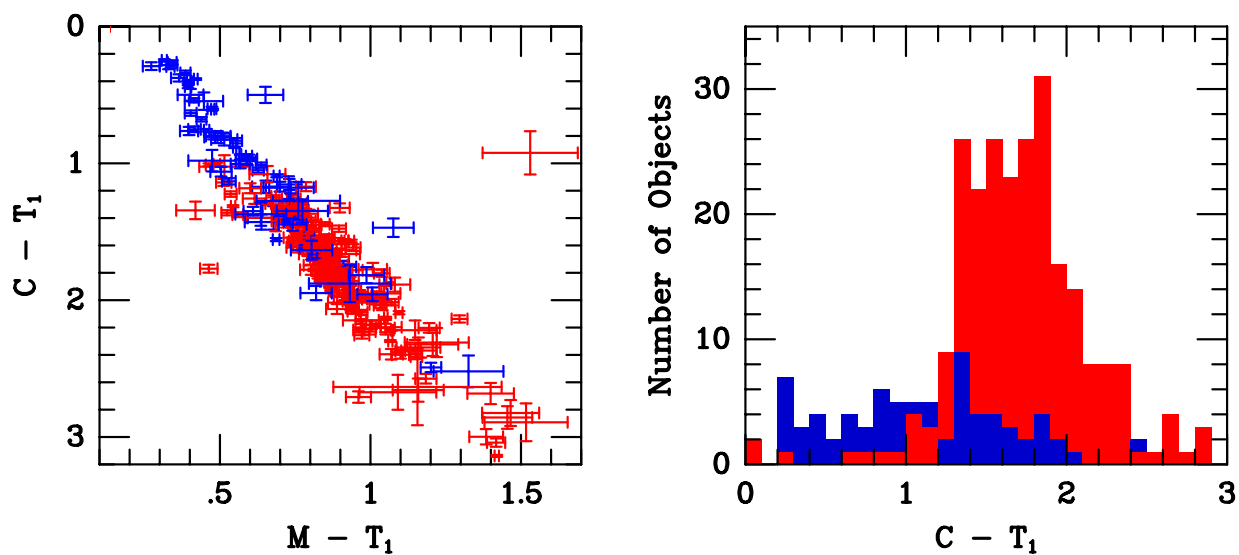


Fig. 6.— Washington system photometry of M31 clusters classified by Caldwell et al. (2009, 2011), with blue representing clusters with ages $t \lesssim 2$ Gyr, and red designating globular clusters, $t \sim 14$ Gyr. On the left is a two-color diagram; on the right is a histogram of $C - T_1$ colors. In the absence of a spectroscopic or *HST* imaging age designation, we classify systems with $C - T_1 < 1.2$ as young, and $C - T_1 > 1.2$ as old.

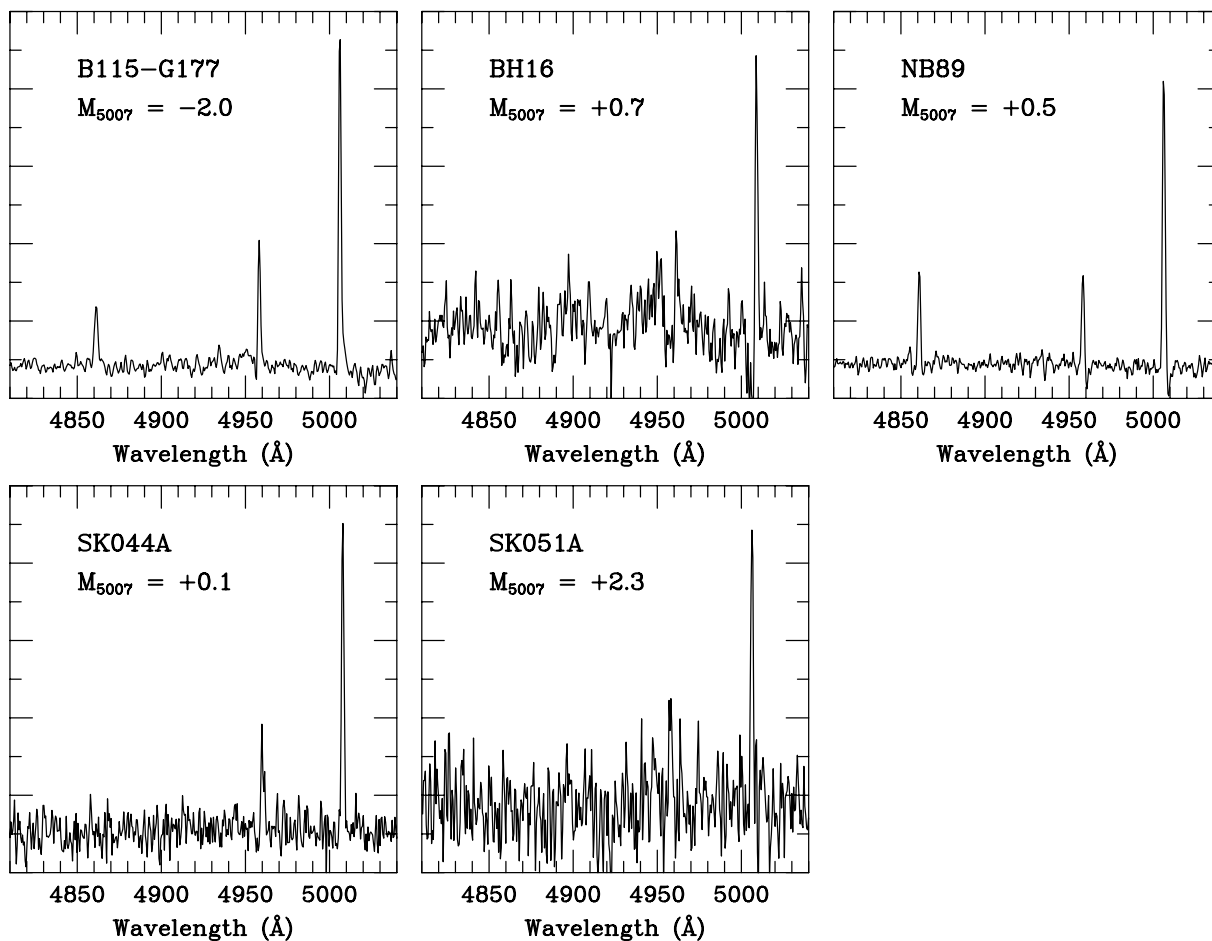


Fig. 7.— The spectra of 5 systems with candidate planetary nebulae in the wavelength range between 4800 Å and 5100 Å. The top three panels show confirmed globular clusters; the bottom two panels show objects which may be globulars. To enhance the visibility of the emission lines, the spectrum of a template globular cluster has been subtracted from each object. The y-axis represents counts; to convert to relative flux, note that the system response at H β is roughly a factor of 1.46 less than that at [O III] λ 5007. For each candidate, the [O III] line is at least twice the strength of H β .

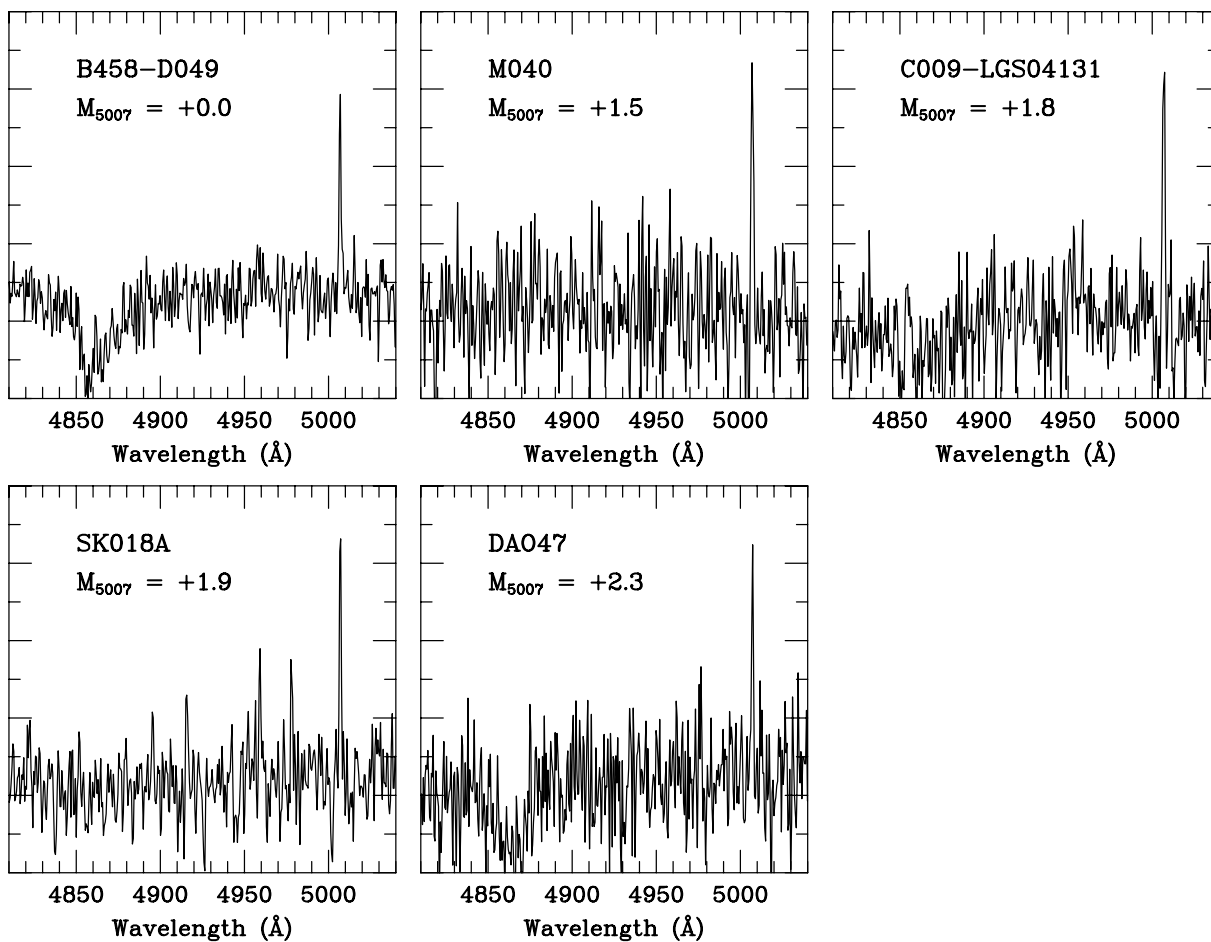


Fig. 8.— The spectra of 5 M31 young clusters in the wavelength range between 4800 Å and 5100 Å. To enhance the visibility of the emission lines, the spectrum of a template young cluster been subtracted from each object; in some cases, a mismatch in age has resulted in a poor subtraction around H β . The y-axis represents counts; to convert to relative flux, note that the response at H β is roughly 1.46 times less than that at [O III] λ 5007. For each candidate, the [O III] line is at least twice the strength of H β .

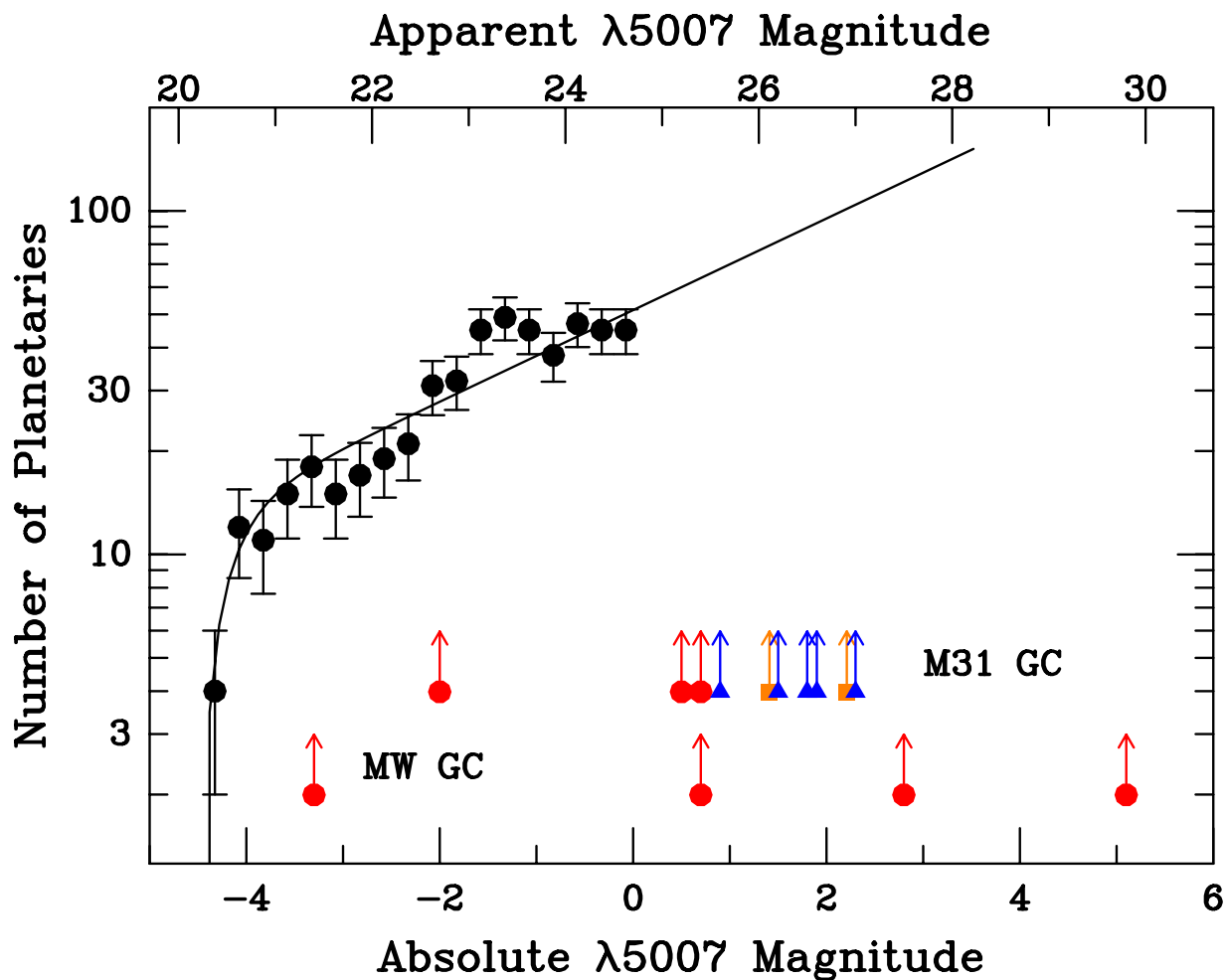


Fig. 9.— The planetary nebula luminosity function for the bulge of M31 (black points with error bars). These data, which extend over nearly 5 magnitudes, represent the deepest M31 PNLF currently available. The solid line shows the model PNLF (an exponential with a bright-end cutoff) that was adopted by Ciardullo et al. (1989). The magnitudes of the clusters PNe are marked: Milky Way PNe on the lower row, and M31 PNe on the upper row. The red circles, blue triangles, and tan squares represent PN candidates in old confirmed clusters, young clusters, and candidate globular clusters, respectively.

Table 1. Log of Hydra Setups

Setup	UT Date	Exposure Times (minutes)	Number of Targets	
			GCs	Young Clusters
M31-Y1	2008 Oct 25	7×30	71	2
M31-Y2	2008 Oct 25	7×30	68	1
M31-Y3	2008 Oct 26	7×30	57	8
M31-Y4	2008 Oct 26	7×30	43	18
M31-B1	2008 Oct 27	7×30	31	25
M31-G1	2008 Oct 27	6×30	37	23
M31-B2	2008 Oct 28	7×30	21	26
M31-R2	2008 Oct 28	7×30	16	6

Table 2. Globular Clusters with Discrepant Velocities

Cluster	T_1	Our v (km s $^{-1}$)	Published v (km s $^{-1}$)	Source ^a	Difference (σ)
B034D	17.69	-37 ± 29	-347 ± 25	1	8.1
B079D	17.89	-89 ± 29	-394 ± 25	1	7.9
B104-NB5	16.29	-288 ± 27	32.9 ± 0.7	2	12.0
B159	18.67	-166 ± 33	-526.0 ± 0.5	2	10.8
B451-D037	17.75	-29 ± 18	-514 ± 12	3	22.3
BH16	17.16	-248 ± 27	-99.9 ± 1.1	2	5.3
NB21-AU5	17.22	-343 ± 43	-748.6 ± 1.8	2	9.4
SK006A	18.81	-25 ± 38	-320 ± 54	4	4.5
SK021A	18.25	-509 ± 30	-223 ± 39	4	5.8
SK026A	18.90	-62 ± 33	-568 ± 55	4	7.9
SK045A	15.50	$+46 \pm 7$	-544 ± 52	4	11.2
SK064A	19.30	-35 ± 16	-259 ± 42	4	4.9
SK079A	18.02	-75 ± 22	-258 ± 26	4	5.3
SK094A	18.16	-158 ± 21	-8 ± 29	4	4.2
SK096A	17.94	-55 ± 9	-313 ± 52	4	4.9
SK104A	17.37	-171 ± 10	-301 ± 17	4	6.6
SK106A	18.94	-158 ± 31	-890 ± 38	4	14.9

^aREFERENCES: (1) Galleti et al. (2006); (2) Strader et al. (2011); (3) Perrett et al. (2002); (4) Kim et al. (2007)

Table 3. Globular Cluster Observations

Name	T_1	$\sigma_{T_1}^a$	C^a	σ_C	M^a	σ_M	Velocity (km s ⁻¹)	σ_V (km s ⁻¹)	Type ^b	Ref ^b	R^c	EW (Å)	Notes
AU010	16.555	0.017	18.325	0.031	17.388	0.019	-311.7	20.1	Old	1	2.8	0.8	
B001-G039	16.395	0.005	18.580	0.013	17.377	0.007	-202.7	10.9	Old	3	
B003-G045	17.151	0.012	18.564	0.014	17.885	0.010	-376.7	13.0	Old	1	
B004-G050	16.452	0.007	18.172	0.010	17.255	0.006	-378.1	5.9	Old	3	
B005-G052	15.045	0.002	16.901	0.004	15.905	0.002	-271.6	14.1	Old	1	
B006-G058	14.967	0.002	16.780	0.003	15.831	0.002	-232.9	6.1	Old	1	
B006D-D036	17.634	0.016	18.386	0.013	18.013	0.013	-538.1	28.1	Young	3	Mean; $\Delta v = 11.6$ km s ⁻¹
B008-G060	16.270	0.006	18.077	0.009	17.103	0.005	-324.6	3.6	Old	1	Mean; $\Delta v = 0.0$ km s ⁻¹
B009-G061	16.379	0.006	17.720	0.006	17.128	0.005	-296.8	11.2	Old	3	
B009D	18.624	0.045	19.574	0.034	19.079	0.030	-518.5	38.5	(Young)	
B010-G062	16.227	0.005	17.722	0.007	16.995	0.005	-165.4	12.7	Old	1	
B011-G063	16.115	0.005	17.538	0.006	16.889	0.004	-243.1	11.3	Old	3	
B012-G064	14.689	0.002	16.097	0.002	15.415	0.002	-360.4	24.5	Old	1	
B012D-D039	18.349	0.031	19.521	0.033	18.966	0.030	-517.8	22.1	Young	3	
B013-G065	16.603	0.007	18.410	0.011	17.473	0.007	-421.1	11.1	Old	1	
B014D	18.193	0.030	19.348	0.027	18.887	0.025	-459.3	53.9	Young	1	
B015-V204	17.011	0.009	19.409	0.027	18.074	0.013	-445.7	15.8	Old	3	
B015D-D041	18.046	0.027	19.216	0.024	18.709	0.021	-485.4	26.2	Young	1	
B016-G066	16.975	0.010	18.856	0.017	17.865	0.010	-394.7	6.3	Old	3	
B017-G070	15.336	0.003	17.463	0.005	16.351	0.003	-533.8	9.2	Old	1	0.0	0.0	
B017D	17.579	0.015	18.948	0.020	18.241	0.016	-492.4	13.2	Young	2	
B018-G071	17.027	0.009	18.539	0.014	17.761	0.010	-580.5	15.1	Young	1	
B019-G072	14.454	0.002	16.270	0.002	15.309	0.001	-222.8	6.7	Old	1	
B019D	18.510	0.040	21.030	0.109	19.799	0.054	-406.0	25.1	Young	1	
B020-G073	14.347	0.001	15.960	0.002	15.157	0.001	-350.2	2.8	Old	1	
B020D-G089	16.862	0.022	18.644	0.041	17.753	0.026	-531.6	26.2	Old	1	0.0	0.0	
B021-G075	16.971	0.010	19.008	0.019	17.967	0.011	-433.9	8.0	Old	1	
B022-G074	16.891	0.009	18.181	0.009	17.630	0.008	-452.9	18.7	Old	3	
B022D	17.928	0.059	18.913	0.055	18.263	0.042	-348.6	18.5	Star?	3	
B023-G078	13.579	0.001	15.799	0.002	14.613	0.001	-445.9	4.3	Old	1	Mean; $\Delta v = 3.5$ km s ⁻¹
B024-G082	16.308	0.004	18.045	0.009	17.098	0.005	-211.6	16.0	Old	3	
B025-G084	16.223	0.006	17.898	0.009	17.049	0.007	-209.0	11.4	Old	1	
B025D-V217	17.112	0.027	19.406	0.077	18.195	0.037	-518.7	54.9	Galaxy	3	Probable M31 cluster ⁱ
B026-G086	16.857	0.009	18.823	0.015	17.768	0.009	-255.2	6.3	Old	1	

Table 3—Continued

Name	T_1	$\sigma_{T_1}^a$	C^a	σ_C	M^a	σ_M	Velocity (km s ⁻¹)	σ_V (km s ⁻¹)	Type ^b	Ref ^b	R^c	EW (Å)	Notes
B026D-V216	17.265	0.016	19.970	0.050	18.322	0.020	-478.4	45.0	Galaxy	3	Probable M31 cluster ⁱ
B027-G087	15.119	0.002	16.650	0.003	15.886	0.003	-291.4	13.8	Old	1	
B028-G088	16.369	0.007	17.773	0.008	17.089	0.007	-410.8	16.5	Old	1	
B029-G090	16.109	0.006	17.677	0.007	17.009	0.007	-505.6	11.1	Old	1	
B030-G091	16.763	0.010	20.151	0.055	18.134	0.017	-386.2	27.4	Old	1	
B031-G092	17.173	0.015	19.568	0.036	18.205	0.018	-319.7	19.2	Old	1	
B032-G093	16.944	0.024	19.289	0.069	18.067	0.033	-527.6	8.1	Old	3	
B032D	(18.366)	...	(19.724)	...	(18.943)	...	-335.5	37.5	Young	1	
B033-G095	17.397	0.018	19.109	0.025	18.258	0.020	-452.3	19.9	Old	1	
B034-G096	14.891	0.002	16.705	0.003	15.727	0.002	-552.5	8.1	Old	3	
B034D	17.694	0.023	21.213	0.144	19.024	0.037	-37.5	29.1	Star	3	
B035	18.809	0.016	20.135	0.029	19.670	0.022	-44.7	6.2	Old	1	
B035D	17.790	0.052	19.189	0.068	18.432	0.048	-358.9	31.4	Young	2	
B036	18.741	0.015	20.487	0.038	19.524	0.020	-507.9	4.9	Old	1	
B037-V327	15.643	0.007	19.715	0.087	17.577	0.020	-331.6	6.1	Old	1	Mean; $\Delta v = 3.1$ km s ⁻¹
B038-G098	15.934	0.010	17.635	0.017	16.772	0.011	-180.7	24.2	Old	1	
B039-G101	15.357	0.006	17.769	0.018	16.473	0.008	-245.4	7.6	Old	1	
B040-G102	16.959	0.013	17.560	0.007	17.397	0.009	-420.6	38.3	Young	1	
B041-G103	17.946	0.060	18.970	0.058	18.424	0.048	-389.5	10.9	Old	1	Mean; $\Delta v = 5.9$ km s ⁻¹
B041D	17.394	0.036	19.704	0.100	18.578	0.053	-235.3	36.8	Old	1	
B042-G104	15.360	0.006	18.401	0.030	16.741	0.010	-299.4	9.1	Old	1	
B042D	17.978	0.061	19.726	0.107	18.762	0.782	-517.6	25.4	Galaxy	3	Probable M31 cluster ⁱ
B043-G106	16.630	0.009	17.070	0.005	16.988	0.007	-422.8	50.3	Young	1	
B043D-V246	16.325	0.013	19.148	0.058	17.569	0.021	-349.5	40.8	Galaxy	3	Probable M31 cluster ⁱ
B044-G107	16.108	0.011	18.288	0.029	17.075	0.014	-273.4	5.8	Old	1	
B044D-V228	17.885	0.027	23.123	0.716	19.502	0.055	Galaxy	3	0.2	0.2	Galaxy ^d
B045-G108	17.201	0.004	18.762	0.009	18.029	0.006	-423.5	6.0	Old	1	
B045D	18.189	0.073	20.823	0.270	19.309	0.102	-313.8	10.7	Old	1	
B046-G109	17.655	0.017	18.912	0.035	18.234	0.021	-376.2	16.1	Old	3	
B046D	(19.620)	...	(18.588)	...	(19.315)	...	-328.7	20.9	Star	3	
B047-G111	18.904	0.017	20.075	0.028	19.654	0.022	-301.2	12.3	Old	3	
B048-G110	15.933	0.010	17.789	0.019	16.817	0.011	-239.9	9.3	Old	1	
B049-G112	17.145	0.015	18.195	0.012	17.735	0.013	-446.4	62.3	Young	1	1.5	0.5	
B050-G113	18.225	0.010	19.791	0.021	18.992	0.013	-109.5	9.4	Old	1	

Table 3—Continued

Name	T_1	σ_{T_1} ^a	C^a	σ_C	M^a	σ_M	Velocity (km s ⁻¹)	σ_V (km s ⁻¹)	Type ^b	Ref ^b	R^c	EW (Å)	Notes
B051-G114	17.440	0.005	19.391	0.015	18.424	0.008	-263.8	5.3	Old	1	
B053	17.685	0.047	19.253	0.071	18.315	0.043	-15.1	9.8	Star	3	
B054-G115	17.399	0.018	19.328	0.030	18.259	0.020	-427.5	20.1	Old	3	
B054D-NB33	17.226	0.031	18.872	0.050	17.853	0.028	-135.0	45.7	Star	3	0.8	0.4	
B055-G116	15.938	0.010	18.511	0.034	17.085	0.014	-320.3	5.2	Old	1	0.0	0.0	Mean; $\Delta v = 0.7$ km s ⁻¹
B056-G117	16.603	0.009	18.684	0.017	17.509	0.010	-371.7	17.9	Old	1	
B057-G118	17.094	0.014	18.448	0.015	17.813	0.013	-437.6	40.5	Old	1	1.4:	0.6	3 components of H β
B058-G119	14.486	0.002	16.005	0.002	15.232	0.002	-218.2	11.1	Old	1	
B059-G120	16.585	0.017	18.615	0.039	17.588	0.022	-289.0	11.0	Old	1	
B060-G121	16.216	0.013	17.533	0.016	16.925	0.013	-527.5	12.7	Old	1	1.0	0.2	
B061-G122	17.883	0.007	19.898	0.023	18.917	0.012	-281.3	9.1	Old	3	
B063-G124	16.928	0.004	19.019	0.011	17.986	0.006	-305.6	7.0	Old	1	
B063D	18.468	0.049	19.062	0.027	18.879	0.036	Star	4	Probable AGN ^e
B064-G125	15.810	0.009	17.234	0.013	16.536	0.009	-315.1	9.9	Old	1	1.0	0.2	
B064D-NB6	15.949	0.010	17.533	0.016	16.674	0.010	20.3	...	Old	1	
B065-G126	16.408	...	17.054	...	(17.165)	...	-399.6	20.5	Old	1	
B066-G128	17.175	0.015	17.514	0.007	17.524	0.011	-423.8	86.4	Young	3	
B067-G129	16.720	0.020	17.979	0.024	17.420	0.019	-347.8	26.2	Old	1	0.7:	0.1	
B068-G130	15.621	0.004	17.991	0.009	16.677	0.005	-326.4	9.1	Old	1	
B069-G132	19.997	0.046	20.543	0.044	20.408	0.043	-234.7	31.6	Young	1	1.0	0.4	
B070-G133	16.372	0.014	17.725	0.019	17.082	0.014	-258.5	32.6	Old	1	
B071	17.294	0.032	19.967	0.123	18.349	0.043	-533.7	30.8	Old	1	1.4	0.4	
B071D	18.399	0.090	19.853	0.124	19.282	0.102	-130.7	36.7	Star	3	2.0	0.9	
B072	18.603	0.013	21.460	0.082	20.021	0.029	-91.4	7.7	Old	1	
B073-G134	15.452	0.003	17.244	0.005	16.273	0.004	-500.9	2.3	Old	1	
B074-G135	18.117	0.009	19.366	0.015	18.821	0.011	-434.6	13.6	Old	1	
B075-G136	16.713	0.019	18.328	0.031	17.435	0.019	-171.8	8.5	Old	1	Mean; $\Delta v = 19.1$ km s ⁻¹
B076-G138	16.243	0.013	17.785	0.020	17.065	0.014	-526.7	9.5	Old	1	0.0	0.0	
B077-G139	16.856	0.022	19.513	0.082	17.978	0.030	-545.2	23.5	Old	1	
B078-G140	17.195	0.029	20.087	0.135	18.675	0.056	-289.0	12.4	Old	1	
B079D	17.889	0.028	20.245	0.066	18.879	0.034	-88.6	29.4	Star	3	
B080-G141	16.730	0.019	19.413	0.075	18.093	0.034	-277.2	9.2	Old	1	
B081-G142	16.470	0.008	17.417	0.006	17.031	0.007	-393.5	37.7	Young	1	0.7	0.2	Mean; $\Delta v = 21.4$ km s ⁻¹
B082-G144	14.617	0.002	17.755	0.007	16.000	0.003	-372.9	8.4	Old	1	

Table 3—Continued

Name	T_1	$\sigma_{T_1}^a$	C^a	σ_C	M^a	σ_M	Velocity (km s ⁻¹)	σ_V (km s ⁻¹)	Type ^b	Ref ^b	R^c	EW (Å)	Notes
B083-G146	16.923	0.009	18.148	0.018	17.422	0.010	-347.2	12.6	Old	1	
B085-G147	16.336	0.007	17.713	0.008	17.051	0.007	-423.0	7.5	Old	1	
B086-G148	14.611	0.003	15.958	0.005	15.327	0.003	-206.7	12.1	Old	1	1.0	0.1	Mean; $\Delta v = 8.2$ km s ⁻¹
B087	19.996	0.045	21.394	0.087	20.645	0.052	-370.8	10.5	Old	3	
B087D	17.084	0.027	18.622	0.041	17.834	0.028	-637.7	18.2	Old	1	1.5	0.7	
B088-G150	16.720	0.003	18.597	0.008	17.745	0.005	-490.6	23.4	Old	1	
B090	17.815	0.053	19.478	0.086	18.643	0.057	-385.3	33.7	Old	1	4.0	0.6	
B090D	16.605	0.018	18.383	0.032	17.372	0.018	-0.6	...	Old	3	3.0	0.5	
B091-G151	17.305	0.034	18.113	0.028	17.760	0.027	-296.7	34.5	Young	3	0.0	0.0	
B091D-D058	16.663	0.003	18.331	0.007	17.505	0.004	-121.1	5.9	Old	1	
B092-G152	16.439	0.015	18.005	0.024	17.221	0.016	-409.2	21.3	Old	1	> 3.5	0.2	
B093-G155	16.241	0.013	18.081	0.025	17.053	0.014	-447.8	12.9	Old	1	
B094-G156	15.001	...	15.805	...	(15.957)	...	-561.9	4.1	Old	1	> 3.0	0.5	
B095-G157	(15.241)	...	(17.361)	...	(16.098)	...	-111.5	6.1	Old	1	0.8	0.1	
B096-G158	15.789	0.008	18.045	0.023	16.724	0.010	-316.6	4.9	Old	1	0.7	0.6	Mean; $\Delta v = 3.9$ km s ⁻¹
B096D	17.592	0.025	19.555	0.036	18.862	0.036	-201.6	24.6	Star	3	0.0	0.0	
B097-G159	18.206	0.010	20.066	0.026	19.103	0.014	-275.0	4.8	Old	1	
B097D	17.869	0.027	19.626	0.033	18.743	0.027	-317.6	25.4	Young	3	1.5	1.7	
B098	15.712	0.004	17.416	0.006	16.500	0.004	-311.9	3.2	Old	1	
B099-G161	16.249	0.013	17.799	0.020	17.051	0.014	-159.3	35.4	Old	1	1.0	0.4	
B100-G163	17.191	0.015	18.940	0.022	18.011	0.016	-433.3	6.2	Old	3	
B101-G164	16.399	0.015	17.922	0.022	17.128	0.015	-362.0	7.1	Old	1	3.0	0.3	
B102	18.196	0.010	19.052	0.012	18.754	0.011	-216.1	12.5	Star	3	
B103-G165	14.634	0.003	16.627	0.008	15.578	0.004	-363.4	7.6	Old	1	
B103D-G245	16.938	0.014	18.737	0.018	17.818	0.014	-156.2	9.8	Old	3	2.0	0.1	
B104-NB5	16.288	0.013	17.846	0.021	17.063	0.014	-288.0	26.8	Old	1	1.4	0.4	
B105-G166	18.622	0.014	20.184	0.030	19.429	0.018	-246.2	9.8	Old	3	0.0	0.0	
B106-G168	15.505	0.007	17.334	0.013	16.345	0.008	-95.4	10.6	Old	1	0.0	0.0	Mean; $\Delta v = 8.2$ km s ⁻¹
B107-G169	15.263	0.005	17.091	0.011	16.144	0.007	-330.5	9.2	Old	1	2.0	0.4	
B109-G170	15.809	0.009	17.816	0.020	16.701	0.010	-601.3	10.2	Old	1	0.0	0.0	
B110-G172	14.647	0.003	16.354	0.006	15.430	0.004	-237.6	8.1	Old	1	> 2.0	0.1	
B111-G173	16.286	0.007	17.732	0.008	17.020	0.007	-408.7	10.7	Old	1	> 2.0	0.1	
B111D-D065	17.590	0.026	17.880	0.010	17.825	0.015	-123.4	34.0	Young	1	0.0	0.0	
B112-G174	15.612	0.007	17.702	0.018	16.547	0.009	-283.4	14.5	Old	1	

Table 3—Continued

Name	T_1	σ_{T_1} ^a	C^a	σ_C	M^a	σ_M	Velocity (km s ⁻¹)	σ_V (km s ⁻¹)	Type ^b	Ref ^b	R^c	EW (Å)	Notes
B112D-M27	18.327	0.041	19.756	0.038	18.929	0.032	-300.1	16.2	Young	2	0.5	0.8	
B114-G175	16.595	0.018	17.963	0.023	17.355	0.018	-292.9	33.9	Old	1	0.7	0.3	
B115-G177	15.390	0.006	17.445	0.014	16.288	0.007	-564.5	28.2	Old	1	3.0	2.5	
B116-G178	17.908	0.007	20.045	0.025	19.168	0.014	-341.3	6.0	Old	1	Mean; $\Delta v = 4.8$ km s ⁻¹
B117-G176	15.910	...	16.677	...	(16.669)	...	-523.3	19.7	Old	1	> 2.0	0.3	
B118D-M049	(17.816)	...	(19.552)	...	(18.532)	...	-202.4	58.9	Young	1	1.5	1.6	
B119-NB14	16.887	0.023	18.662	0.041	17.859	0.028	-334.4	25.3	Old	1	0.7	0.5	
B122-G181	18.787	0.015	21.612	0.094	20.217	0.034	-433.4	10.5	Old	3	
B123-G182	16.677	0.019	18.366	0.032	17.477	0.020	-370.7	6.5	Old	1	1.5	0.4	
B124-NB10	14.122	0.002	16.018	0.005	14.969	0.003	-67.7	15.5	Old	1	0.6	0.1	Mean; $\Delta v = 3.7$ km s ⁻¹
B125-G183	15.998	0.010	17.361	0.014	16.701	0.010	-661.1	15.5	Old	1	0.7	0.2	
B126-G184	16.514	0.016	17.965	0.023	17.286	0.017	-168.4	...	Old	1	0.0	0.0	
B127-G185	13.784	0.002	15.611	0.004	14.635	0.002	-506.4	8.1	Old	1	1.5	0.8	
B128-G187	16.357	0.014	18.190	0.027	17.196	0.016	-379.9	6.3	Old	1	3.1	0.2	Mean; $\Delta v = 0.3$ km s ⁻¹
B129	18.072	0.008	22.425	0.171	19.963	0.026	-53.5	7.9	Old	1	> 1.8	0.4	
B130-G188	18.174	0.009	19.977	0.024	19.175	0.015	-32.4	14.0	Old	1	
B131-G189	14.920	0.004	16.638	0.008	15.721	0.005	-450.4	21.5	Old	1	
B134-G190	15.931	0.010	17.498	0.016	16.642	0.010	-359.8	11.4	Old	1	1.8	0.4	
B135-G192	17.358	0.005	18.924	0.011	18.237	0.007	-373.2	23.1	Old	1	> 6.0	0.6	
B137-G195	18.988	0.018	21.207	0.069	20.100	0.031	-225.6	12.9	Old	3	
B141-G197	18.252	0.010	19.868	0.023	19.158	0.015	-172.9	12.3	Old	1	0.0	0.0	
B143-G198	15.379	0.006	17.341	0.013	16.283	0.007	-154.3	7.5	Old	1	0.9	0.1	
B144	16.062	0.011	18.036	0.024	16.942	0.012	-58.0	62.7	Old	1	1.3	0.7	
B145	17.497	0.040	18.841	0.050	17.880	0.029	-323.3	13.4	Old	1	0.7	< 0.1	
B146	16.279	0.013	18.104	0.025	17.124	0.015	-57.6	28.5	Old	1	0.0	0.0	
B147-G199	15.063	0.004	16.894	0.009	15.852	0.005	-95.1	10.2	Old	1	
B148-G200	15.354	0.006	16.956	0.010	16.120	0.006	-314.4	12.7	Old	1	2.2	0.5	$R = 0.7$ for 2nd component
B149-G201	18.322	0.011	20.092	0.027	18.748	0.011	-58.1	28.4	Old	1	
B150-G203	16.045	0.011	18.007	0.023	16.941	0.013	-150.5	18.1	Old	1	0.9	0.4	
B151-G205	14.163	0.002	16.462	0.007	15.193	0.003	-340.8	6.5	Old	1	
B152-G207	15.540	0.007	17.340	0.013	16.385	0.008	-148.0	8.6	Old	1	0.7	0.1	
B153	15.637	0.007	17.547	0.016	16.469	0.008	-249.9	3.3	Old	1	1.8	0.2	Mean; $\Delta v = 0.3$ km s ⁻¹
B154-G208	16.373	0.014	18.437	0.033	17.225	0.016	-226.6	7.2	Old	1	1.0	0.3	
B155-G210	17.290	0.032	19.308	0.072	18.192	0.038	-416.6	12.2	Old	1	1.0	0.3	

Table 3—Continued

Name	T_1	$\sigma_{T_1}^a$	C^a	σ_C	M^a	σ_M	Velocity (km s ⁻¹)	σ_V (km s ⁻¹)	Type ^b	Ref ^b	R^c	EW (Å)	Notes
B156-G211	16.459	0.015	17.902	0.022	17.179	0.016	-374.2	5.4	Old	1	
B158-G213	14.142	0.002	15.833	0.004	14.930	0.003	-186.1	4.0	Old	1	Mean; $\Delta v = 5.7$ km s ⁻¹
B159	18.674	0.014	20.872	0.051	19.689	0.022	-166.3	33.1	Old	1	1.1	0.7	
B160-G214	17.552	0.042	18.631	0.043	18.174	0.038	-357.9	18.4	Old	1	
B161-G215	15.883	0.009	17.404	0.014	16.625	0.010	-442.4	5.8	Old	1	Mean; $\Delta v = 0.7$ km s ⁻¹
B162-G216	16.881	0.013	18.868	0.019	17.840	0.015	-149.3	11.2	Old	1	1.4	0.3	
B163-G217	14.428	0.002	16.467	0.003	15.334	0.002	-163.4	4.2	Old	1	
B164-V253	17.295	0.016	19.272	0.024	18.165	0.016	+35.9	15.7	Old	1	0.0	0.0	Mean; $\Delta v = 5.5$ km s ⁻¹
B165-G218	16.080	0.006	17.321	0.005	16.722	0.005	-74.6	18.5	Old	1	
B167	16.788	0.010	18.828	0.016	17.692	0.011	-213.7	9.0	Old	1	0.7	0.2	
B168	17.108	0.016	20.106	0.054	18.456	0.024	-181.7	26.8	Old	1	
B169	16.645	0.009	18.863	0.016	17.570	0.010	-160.5	18.8	Old	1	
B170-G221	16.849	0.006	18.608	0.012	17.656	0.008	-291.8	2.8	Old	1	Mean; $\Delta v = 2.3$ km s ⁻¹
B171-G222	14.756	0.002	16.691	0.003	15.590	0.002	-267.5	5.4	Old	1	
B173-G224	17.389	0.017	19.592	0.031	18.548	0.022	-193.2	31.4	Old	1	> 2.0	0.5	
B174-G226	14.879	0.002	16.809	0.004	15.807	0.003	-490.8	12.8	Old	1	
B176-G227	16.124	0.003	17.454	0.005	16.806	0.004	-532.7	12.4	Old	1	Mean; $\Delta v = 2.8$ km s ⁻¹
B178-G229	14.632	0.002	16.077	0.002	15.326	0.002	-156.2	14.1	Old	1	
B179-G230	14.917	0.002	16.521	0.003	15.649	0.002	-150.2	11.0	Old	1	
B180-G231	15.596	0.004	17.353	0.005	16.404	0.004	-198.2	2.6	Old	1	Mean; $\Delta v = 0.7$ km s ⁻¹
B182-G233	14.895	0.002	16.751	0.003	15.754	0.002	-355.1	2.2	Old	1	Mean; $\Delta v = 1.0$ km s ⁻¹
B183-G234	15.478	0.003	17.349	0.005	16.294	0.003	-188.2	7.9	Old	1	
B184-G236	16.632	0.011	18.862	0.019	17.591	0.012	-155.4	14.1	Old	3	
B185-G235	15.079	0.002	16.898	0.003	15.864	0.002	-156.4	3.7	Old	1	Mean; $\Delta v = 2.1$ km s ⁻¹
B187-G237	16.500	0.009	18.485	0.014	17.497	0.011	-88.0	10.2	Old	1	> 1.6	0.1	
B188-G239	16.617	0.011	18.061	0.010	17.430	0.010	-212.1	17.6	Old	1	0.0	0.0	
B189-G240	16.459	0.009	18.615	0.015	17.391	0.010	-137.7	17.5	Old	3	
B190-G241	16.286	0.008	17.958	0.009	17.135	0.008	-91.6	9.9	Old	1	2.0	0.1	
B192-G242	18.035	0.040	18.534	0.016	18.401	0.025	-147.0	29.8	Young	3	1.1	0.7	
B193-G244	14.795	0.002	16.820	0.004	15.701	0.003	-62.7	2.2	Old	1	
B194-G243	16.753	0.010	18.185	0.010	17.441	0.009	-398.6	8.2	Old	1	Mean; $\Delta v = 2.8$ km s ⁻¹
B196D-SH08	(18.667)	...	(20.560)	...	(19.441)	Young	3	0.1	0.8	
B197-G247	17.056	0.015	19.259	0.027	18.069	0.018	-68.1	5.8	Old	3	
B198-G249	17.157	0.017	18.632	0.017	17.926	0.016	-30.0	20.0	Old	3	1.3	0.3	

Table 3—Continued

Name	T_1	$\sigma_{T_1}^a$	C^a	σ_C	M^a	σ_M	Velocity (km s^{-1})	σ_V (km s^{-1})	Type ^b	Ref ^b	R^c	EW (\AA)	Notes
B199-G248	17.109	0.007	18.442	0.011	17.796	0.009	-365.9	12.3	Old	1	
B200	17.824	0.031	19.775	0.044	18.833	0.036	-120.4	21.3	Old	3	1.3	0.4	
B201-G250	15.679	0.004	17.233	0.005	16.414	0.004	-713.0	5.8	Old	1	2.8	0.1	
B201D-D044	(18.104)	...	(20.118)	...	(18.923)	...	-490.5	38.6	Young	3	
B203-G252	16.118	0.007	17.840	0.008	16.960	0.007	-223.9	6.4	Old	1	
B204-G254	15.228	0.003	17.011	0.004	16.004	0.003	-352.7	12.1	Old	1	
B205-G256	14.912	0.002	16.534	0.003	15.711	0.003	-371.1	10.8	Old	1	
B206-G257	14.535	0.002	16.115	0.002	15.314	0.002	-194.3	8.7	Old	1	
B206D-D048	18.142	0.036	18.967	0.024	18.620	0.028	-489.0	31.0	Young	3	0.9	0.3	
B207-G258	16.904	0.011	18.322	0.011	17.573	0.010	-162.7	7.6	Old	1	
B208-G259	17.194	0.018	19.165	0.025	18.131	0.019	-244.1	12.0	Old	1	
B209-G261	16.093	0.007	17.642	0.007	16.858	0.006	-453.7	11.4	Old	1	
B210-M11	17.176	0.014	18.188	0.010	17.777	0.012	-254.2	61.4	Young	3	
B211-G262	16.222	0.006	17.576	0.006	16.898	0.006	-161.9	13.2	Old	1	
B212-G263	15.060	0.002	16.440	0.003	15.737	0.002	-403.0	21.4	Old	1	
B213-G264	16.337	0.008	18.157	0.011	17.198	0.008	-569.6	5.7	Old	1	
B214-G265	17.112	0.012	18.590	0.020	17.972	0.020	-271.4	18.9	Old	3	0.0	0.0	
B215-G266	16.670	0.011	18.512	0.014	17.478	0.011	-152.2	10.7	Old	1	
B215D-D056	16.164	0.012	17.144	0.012	16.691	0.010	-35.7	68.2	Star	3	
B217-G269	15.955	0.006	17.727	0.008	16.781	0.006	-21.3	7.9	Old	1	
B218-G272	14.302	0.002	15.977	0.002	15.057	0.001	-219.5	13.7	Old	1	
B219-G271	15.901	0.003	17.710	0.006	16.713	0.004	-505.7	4.8	Old	1	Mean; $\Delta v = 3.1 \text{ km s}^{-1}$
B220-G275	16.097	0.007	17.530	0.007	16.834	0.006	-279.5	23.3	Old	1	0.0	0.0	
B221-G276	16.233	0.007	18.011	0.009	17.109	0.008	-459.0	9.9	Old	1	0.7	0.1	
B222-G277	17.059	0.013	18.427	0.012	17.718	0.011	-301.4	19.6	Young	1	
B224-G279	14.983	0.002	16.369	0.003	15.713	0.002	-157.7	12.2	Old	1	
B225-G280	13.637	0.001	15.500	0.001	14.434	0.001	-159.9	3.6	Old	1	
B228-G281	16.211	0.007	18.123	0.010	17.097	0.008	-425.2	13.5	Old	1	
B229-G282	16.133	0.007	17.422	0.006	16.851	0.006	-62.3	19.0	Old	1	
B230-G283	15.593	0.002	16.861	0.003	16.256	0.003	-570.2	12.2	Old	1	0.0	0.0	Mean; $\Delta v = 0.8 \text{ km s}^{-1}$
B231-G285	16.722	0.012	18.344	0.013	17.494	0.011	-292.1	10.5	Old	1	0.0	0.0	
B232-G286	15.237	0.003	16.651	0.003	15.927	0.003	-183.6	22.5	Old	1	
B233-G287	15.286	0.003	16.872	0.004	16.077	0.003	-80.5	20.5	Old	3	
B234-G290	16.241	0.007	17.984	0.009	17.074	0.007	-202.5	8.2	Old	1	0.2	0.2	

Table 3—Continued

Name	T_1	σ_{T_1} ^a	C^a	σ_C	M^a	σ_M	Velocity (km s ⁻¹)	σ_V (km s ⁻¹)	Type ^b	Ref ^b	R^c	EW (Å)	Notes
B235-G297	15.777	0.005	17.414	0.006	16.559	0.005	-92.0	4.2	Old	1	
B237-G299	16.823	0.011	18.249	0.010	17.523	0.009	-117.0	18.9	Old	1	
B238-G301	15.981	0.005	17.758	0.007	16.757	0.005	-43.2	5.5	Old	1	
B239-M74	16.762	0.006	18.285	0.009	17.489	0.007	-236.6	12.4	Old	3	0.0	0.0	
B240D-D066	17.790	0.032	17.512	0.008	17.828	0.016	-106.1	62.6	Young	3	
B246	17.660	0.017	19.281	0.026	18.511	0.020	-477.7	20.8	Old	1	
B247	16.949	0.009	18.491	0.013	17.708	0.010	-508.9	11.4	Young	2	
B248	17.542	0.015	19.206	0.024	18.327	0.017	-554.1	13.7	Old	1	
B248D-D070	17.632	0.026	20.278	0.065	18.808	0.034	-46.6	36.0	Star	3	
B249	17.190	0.011	19.898	0.040	18.114	0.014	-501.6	30.9	Old	3	
B250D-D071	16.573	0.008	19.316	0.075	17.740	0.020	Galaxy	3	Galaxy ^f
B251	17.194	0.015	19.985	0.050	18.306	0.020	-497.6	38.6	Galaxy	3	Probable M31 cluster ⁱ
B253	18.269	0.041	19.229	0.030	18.872	0.035	-467.2	56.0	Star	3	4.3	1.7	
B255D-D072	17.650	0.016	19.360	0.048	18.469	0.024	-114.0	14.1	Old	4	
B257D-D073	17.646	0.016	18.651	0.027	18.177	0.019	-113.8	33.1	Young	2	
B258	17.680	0.047	18.855	0.052	18.361	0.045	-283.8	55.9	(Young)	
B258D	16.322	0.005	19.398	0.044	17.822	0.013	9.5	60.7	Star	3	0.0	0.0	
B262	17.016	0.025	18.650	0.041	17.884	0.029	-268.3	26.6	Old	1	2.4	1.1	
B265	17.949	0.030	19.692	0.042	18.786	0.032	-496.8	4.5	Old	1	Mean; $\Delta v = 11.4$ km s ⁻¹
B271	17.736	0.029	19.693	0.041	18.706	0.032	-166.9	46.3	Intermediate	3	0.7	0.5	
B272-V294	17.506	0.023	19.874	0.046	18.636	0.029	-124.7	9.8	Old	1	
B274	18.081	0.039	20.404	0.075	19.251	0.051	-131.4	26.9	Old	3	0.9	0.5	
B277-M22	18.444	0.045	19.722	0.037	19.142	0.039	-345.0	13.4	Young	2	
B279-D068	17.812	0.031	19.959	0.051	18.744	0.033	-121.9	19.0	Old	3	
B281-G288	17.240	0.015	18.859	0.017	17.991	0.014	-206.3	8.9	Young	2	
B283-G296	17.299	0.016	18.913	0.018	18.100	0.015	-91.7	12.9	Old	1	
B303-G026	17.775	0.015	18.408	0.013	18.142	0.013	-501.7	42.7	Young	3	
B304-G028	16.486	0.005	17.781	0.008	17.110	0.005	-406.5	14.2	Old	3	
B305-D024	17.480	0.015	18.901	0.046	18.165	0.023	-499.7	29.4	Young	2	
B306-G029	15.587	0.002	17.955	0.008	16.692	0.004	-430.3	9.1	Old	3	
B307-G030	16.962	0.009	18.331	0.011	17.683	0.009	-435.0	9.0	Intermediate	3	
B309-G031	17.072	0.016	18.651	0.062	17.824	0.020	-398.4	17.0	Old	3	
B311-G033	14.992	0.002	16.562	0.003	15.790	0.002	-507.8	7.3	Old	3	
B312-G035	15.019	0.002	16.691	0.003	15.832	0.002	-174.5	7.1	Old	3	

Table 3—Continued

Name	T_1	σ_{T_1} ^a	C^a	σ_C	M^a	σ_M	Velocity (km s ⁻¹)	σ_V (km s ⁻¹)	Type ^b	Ref ^b	R^c	EW (Å)	Notes
B313-G036	15.773	0.003	17.661	0.006	16.671	0.004	-427.2	13.4	Old	3	
B315-G038	16.035	0.004	16.640	0.003	16.475	0.003	-556.6	32.9	Young	3	
B316-G040	16.584	0.006	18.005	0.009	17.271	0.007	-366.4	10.4	Intermediate	3	
B318-G042	16.743	0.007	16.991	0.004	17.022	0.005	-552.6	56.2	Young	3	
B319-G044	17.205	0.011	17.609	0.007	17.563	0.008	-572.9	41.9	Young	3	
B321-G046	17.416	0.013	17.956	0.009	17.794	0.010	-520.9	56.1	Young	3	
B322-G049	17.389	0.013	17.651	0.007	17.694	0.009	-568.9	36.6	Young	1	0.0	0.0	
B325	16.670	0.007	17.761	0.007	17.321	0.007	-599.0	19.2	Young	3	
B327-G053	16.323	0.005	16.707	0.003	16.706	0.004	-548.7	33.4	Young	1	0.0	0.0	
B330-G056	17.059	0.010	18.412	0.011	17.802	0.009	-256.4	14.3	Old	3	
B335-V013	17.135	0.010	19.626	0.033	18.299	0.015	-527.7	14.7	Young	1	
B338-G076	13.821	0.001	15.271	0.001	14.538	0.001	-264.7	8.0	Old	3	
B341-G081	15.783	0.003	17.400	0.005	16.556	0.004	-360.7	8.5	Old	1	
B342-G094	17.720	0.011	18.012	0.008	18.019	0.010	-459.3	66.3	Young	3	1.1	0.2	
B343-G105	15.885	0.006	17.245	0.012	16.594	0.007	-360.0	1.7	Old	3	
B344-G127	15.716	0.003	17.030	0.007	16.224	0.004	-243.2	15.8	Old	3	
B345-G143	16.287	0.003	17.617	0.005	16.983	0.004	-354.6	7.8	Old	3	
B347-G154	16.338	0.005	17.349	0.009	16.765	0.006	-263.6	16.7	Old	3	
B348-G153	16.702	0.007	18.077	0.017	17.225	0.009	-187.9	8.2	Old	3	
B350-G162	16.233	0.003	17.551	0.005	16.928	0.004	-413.8	9.8	Old	1	
B352-G180	16.404	0.005	17.411	0.010	16.858	0.006	-292.1	9.5	Old	3	
B354-G186	17.620	0.016	18.802	0.032	18.184	0.020	-162.3	14.9	Old	3	
B355-G193	17.658	0.017	18.422	0.024	17.961	0.017	-77.8	10.6	Star?	3	
B356-G206	16.771	0.007	18.132	0.017	17.258	0.009	-186.2	2.1	Old	3	
B365-G284	16.225	0.006	17.650	0.019	16.948	0.010	-71.0	12.6	Old	3	
B366-G291	15.828	0.003	17.296	0.008	16.593	0.005	-140.7	13.5	Old	3	0.0	0.0	
B368-G293	17.824	0.020	18.107	0.018	18.117	0.019	-156.8	50.0	Young	2	1.4	0.6	
B370-G300	15.746	0.003	17.412	0.008	16.574	0.005	-352.7	11.5	Old	3	0.0	0.0	
B371-G303	17.634	0.013	18.392	0.011	18.053	0.011	-97.0	23.8	Young	3	
B372-G304	16.068	0.004	17.672	0.009	16.829	0.005	-225.8	7.7	Old	3	
B373-G305	15.131	0.002	16.976	0.005	15.966	0.003	-216.2	9.9	Old	3	
B374-G306	17.896	0.017	18.778	0.014	18.408	0.015	-111.0	24.8	Young	3	0.0	0.0	
B375-G307	17.080	0.008	18.859	0.014	17.883	0.009	-196.5	9.4	Old	3	
B376-G309	17.759	0.015	18.437	0.011	18.162	0.012	-137.0	23.1	Young	3	

Table 3—Continued

Name	T_1	$\sigma_{T_1}^a$	C^a	σ_C	M^a	σ_M	Velocity (km s^{-1})	σ_V (km s^{-1})	Type ^b	Ref ^b	R^c	EW (\AA)	Notes
B378-G311	17.182	0.011	18.508	0.020	17.917	0.014	-204.4	29.2	Old	3	
B382-G317	16.939	0.007	18.276	0.009	17.600	0.007	-287.6	11.7	Old	3	
B386-G322	15.142	0.002	16.744	0.004	15.920	0.003	-390.6	9.6	Old	3	
B388	17.684	0.013	20.005	0.036	18.694	0.018	-61.0	36.7	Star	3	
B391-G328	16.779	0.006	18.322	0.009	17.493	0.007	-324.2	10.1	Old	3	
B392-G329	(16.327)	...	(17.884)	...	(16.977)	...	-74.9	15.2	Young	3	
B431-G027	(17.084)	...	(19.539)	...	(18.065)	...	-500.7	56.8	Young	3	
B442-D033	(17.609)	...	(19.008)	...	(18.201)	...	-572.3	48.1	Young	4	
B443-D034	18.154	0.025	18.432	0.014	18.420	0.017	-534.3	25.9	Young	3	
B448-D035	17.368	0.013	18.352	0.012	17.923	0.012	-537.1	19.5	Young	3	Mean; $\Delta v = 11.9 \text{ km s}^{-1}$
B451-D037	17.755	0.018	18.894	0.019	18.316	0.017	-28.9	18.1	Star?	3	
B453-D042	17.926	0.022	18.302	0.012	18.254	0.017	-470.9	43.1	Young	3	
B458-D049	17.552	0.021	18.352	0.014	17.994	0.016	-494.7	39.0	Young	1	2.1	0.8	
B467-G202	17.360	0.013	18.500	0.025	17.836	0.015	-290.3	10.3	Old	3	
B472-D064	14.648	0.002	16.219	0.002	15.436	0.002	-120.5	12.1	Old	1	
B475-V128	17.150	0.011	18.086	0.016	17.682	0.012	-115.6	33.9	Young	3	
B480-V127	17.640	0.016	18.475	0.020	18.158	0.018	-120.7	26.4	Young	3	
B483-D085	17.995	0.022	18.796	0.027	18.468	0.024	-100.3	25.4	Young	3	
B484-G310	17.892	0.020	18.860	0.029	18.444	0.023	-104.9	28.3	Young	3	
BH16	17.164	0.029	18.656	0.042	17.623	0.023	-248.4	27.8	Old	1	4.0	0.7	
BH18	17.384	0.036	19.270	0.070	18.428	0.047	-469.8	20.6	Old	3	1.2	1.1	
C009-LGS04131	(18.699)	...	(19.679)	...	(19.136)	...	-483.5	51.4	Young	3	> 6.0	1.0	
DAO23	18.364	0.025	20.592	0.081	19.579	0.046	-16.2	40.1	(Old)	
DAO30	17.821	0.019	19.169	0.024	18.558	0.019	-465.2	18.9	Young	3	
DAO47	18.494	0.050	19.258	0.031	18.855	0.035	-511.7	31.5	Young	3	3.5	0.5	
DAO84	18.643	0.033	19.143	0.020	19.258	0.032	-210.6	132.3	Young	2	0.3	2.0	
Fan 15	18.310	-307.4	29.3	
Fan 16	18.640	-302.2	24.4	Mean; $\Delta v = 6.7 \text{ km s}^{-1}$
Fan 37	15.290	-344.5	48.0	1.9	0.5	
Fan 42	16.610	-270.8	43.0	1.0	0.3	
Fan 55	18.220	-205.6	38.4	
G083-V225	(18.162)	...	(19.729)	...	(18.816)	...	-337.4	41.7	Young	1	
G137	18.914	0.018	19.170	0.014	19.175	0.015	34.1	...	Old	3	2.9	370	PN
KHM31-81	(19.302)	...	(20.433)	...	(19.795)	...	-511.8	52.5	Young	3	0.0	0.0	

Table 3—Continued

Name	T_1	$\sigma_{T_1}^a$	C^a	σ_C	M^a	σ_M	Velocity (km s ⁻¹)	σ_V (km s ⁻¹)	Type ^b	Ref ^b	R^c	EW (Å)	Notes
M009	17.306	0.016	18.661	0.015	18.019	0.014	-335.1	24.4	Old	3	0.7	0.6	
M019	17.772	0.030	19.340	0.031	18.628	0.030	-247.6	14.5	Old	3	
M028	18.316	0.051	19.234	0.030	18.811	0.037	-92.5	16.7	Star	4	
M040	18.393	0.053	20.210	0.066	19.344	0.057	-189.7	38.2	Young	2	4.1	1.6	
M043	19.337	0.102	20.709	0.090	19.936	0.080	-190.7	46.2	Young	2	
M045	18.131	0.042	20.010	0.055	19.026	0.043	-176.3	29.9	Young	2	
M047	18.237	0.046	19.872	0.049	19.005	0.042	-80.2	16.4	Intermediate	1	0.0	0.0	
M058	17.885	0.034	19.356	0.032	18.925	0.039	-145.6	19.4	Young	2	
M059	18.219	0.027	19.666	0.065	18.924	0.037	-89.8	20.0	Young	3	
M094	19.666	0.101	20.753	0.158	20.354	0.130	-209.3	21.7	Star	4	0.0	0.0	
MITA140	(16.059)	...	(19.960)	...	(17.574)	...	-328.1	19.0	Old	1	
MITA166	18.230	-323.7	35.8	> 1.8	0.4	
NB16	17.491	0.039	19.585	0.092	18.486	0.049	-197.9	24.0	Old	3	> 4.0	0.7	
NB17-AU014	19.060	0.167	20.033	0.152	19.548	0.134	-308.9	43.1	Old	4	1.3	0.8	
NB21-AU5	17.224	0.031	19.095	0.060	17.940	0.030	-343.3	43.2	Old	1	0.4	0.3	
NB23	16.665	0.019	18.570	0.038	17.519	0.021	-320.9	23.8	Galaxy	3	2.8	1.0	FWHM = 262 km s ⁻¹
NB63	16.788	0.021	17.955	0.024	17.296	0.018	-114.9	18.4	Star?	3	1.0	0.4	
NB67-AU13	15.564	0.007	16.559	0.008	16.064	0.006	-23.4	17.2	Star	3	
NB89	(17.423)	...	(19.433)	...	(18.240)	...	-350.2	30.1	Old	4	2.1	1.5	
PHF7-2	(17.773)	...	(19.123)	...	(18.347)	...	-538.7	28.4	Young	1	
SK006A	18.811	0.045	20.267	0.063	19.459	0.043	-24.6	38.5	Star	4	
SK007A	17.630	0.017	17.563	0.007	17.834	0.012	-436.9	45.6	Young	4	
SK008A	18.581	0.038	20.209	0.059	19.350	0.042	-58.8	21.8	Star	3	
SK009A	19.374	0.079	20.838	0.106	20.260	0.097	-415.8	23.6	Star	4	
SK010A	18.154	0.025	19.519	0.032	19.116	0.031	-556.6	24.4	Star	4	
SK012A	18.125	0.025	20.022	0.049	18.964	0.030	-404.5	19.7	Star	4	
SK013A	18.568	0.038	20.399	0.069	19.423	0.045	-64.1	67.7	Star	4	
SK014A	17.460	0.014	18.449	0.013	17.955	0.013	-484.7	44.0	Star	4	2.2	3.4	
SK015A	19.716	0.110	20.524	0.085	20.416	0.114	-542.0	33.1	(Young)	...	0.3	0.5	
SK016A	19.259	0.070	21.578	0.194	20.275	0.096	-546.2	26.8	(Young)	...	0.5	0.5	
SK017A	18.867	0.050	19.830	0.045	19.322	0.042	-485.0	17.3	Star	4	
SK018A	18.701	0.048	19.975	0.047	19.425	0.040	-345.3	14.9	Young	3	> 4.0	1.2	Mean; $\Delta v = 6.5$ km s ⁻¹
SK019A	18.225	0.029	20.675	0.073	19.283	0.031	Old	4	
SK021A	18.251	0.040	19.963	0.054	19.191	0.045	-508.7	29.7	Star	4	0.4	0.3	

Table 3—Continued

Name	T_1	$\sigma_{T_1}^a$	C^a	σ_C	M^a	σ_M	Velocity (km s ⁻¹)	σ_V (km s ⁻¹)	Type ^b	Ref ^b	R^c	EW (Å)	Notes
SK022A	18.631	0.025	19.960	0.037	19.391	0.031	-475.2	19.0	Star	4	
SK023A	18.976	0.078	20.216	0.071	19.920	0.089	-537.7	76.1	Star	4	0.0	0.0	
SK024A	18.987	0.034	21.844	0.181	20.039	0.055	-462.8	22.6	Star	4	
SK025A	19.321	0.104	22.211	0.381	20.697	0.173	-551.6	22.5	Star	4	
SK026A	18.904	0.032	20.941	0.085	19.685	0.040	-61.8	32.7	Old	4	
SK027A	19.167	0.092	20.893	0.126	20.198	0.113	-487.4	24.3	Star	4	> 1.5	0.4	
SK028A	18.832	0.066	21.565	0.213	20.367	0.127	-473.9	31.0	Star	4	
SK029A	18.718	0.061	20.095	0.063	19.473	0.059	-464.3	32.5	Star	4	
SK030A	18.882	0.071	20.528	0.091	19.621	0.068	-565.8	27.2	Star	4	2.2	0.9	
SK031A	19.530	0.128	21.179	0.165	20.648	0.171	-518.9	38.3	Star	3	
SK032A	18.749	0.063	20.239	0.071	19.378	0.055	-472.2	28.9	Star	4	
SK033A	19.017	0.081	20.162	0.068	19.759	0.078	-454.6	43.5	Star	4	0.9	0.9	
SK037A	19.896	0.183	20.412	0.090	20.356	0.137	-417.2	76.2	Star	4	1.5	0.9	
SK039A	18.114	0.070	19.249	0.074	18.695	0.061	-125.6	17.7	Star	4	1.5	0.7	
SK040A	18.802	0.066	20.280	0.073	19.486	0.060	-466.4	58.3	Star	4	> 2.0	1.9	
SK041A	18.910	0.074	19.615	0.043	19.291	0.052	-441.0	64.0	Star	4	3.6	2.2	
SK042A	19.614	0.140	20.379	0.086	20.618	0.170	-546.8	78.1	HII	4	0.8	4.2	
SK043A	18.493	0.049	20.273	0.071	19.397	0.055	-121.4	51.7	Star	4	> 3.0	0.9	
SK044A	18.328	0.043	19.466	0.036	19.158	0.045	-518.4	39.0	Star	4	> 12.0	5.0	
SK045A	15.497	0.003	16.946	0.004	16.153	0.003	45.7	7.1	Star	4	
SK046A	18.975	0.077	20.264	0.074	19.678	0.072	-503.9	14.4	Star	4	
SK047A	19.681	0.148	20.865	0.128	20.311	0.129	-380.0	91.4	Star	4	2.1	1.5	
SK048A	18.129	0.036	19.345	0.032	18.840	0.034	-427.1	79.0	Star	4	4.0	2.4	
SK049A	19.378	0.112	20.919	0.131	20.200	0.115	Old	4	> 4.0	3.6	
SK050A	17.508	0.040	19.384	0.078	18.399	0.046	-328.6	25.4	Star	4	1.3	0.5	
SK051A	18.869	0.069	21.305	0.173	20.075	0.099	-365.5	22.1	Star	4	> 5.0	1.5	
SK052A	18.186	0.027	19.321	0.052	18.777	0.034	-75.6	16.6	Old	4	
SK053A	17.858	0.013	19.571	0.025	18.643	0.016	-380.2	8.8	Old	4	
SK054A	17.702	0.048	19.380	0.079	18.461	0.049	-614.1	38.6	Old	4	0.0	0.0	
SK055A	18.074	0.034	19.808	0.047	18.861	0.034	Old	4	
SK056A	18.405	0.046	19.853	0.050	19.011	0.039	-422.1	84.6	HII	4	2.0	0.6	
SK058A	18.945	0.054	19.800	0.082	19.593	0.073	-246.7	23.2	Star	4	
SK059A	17.111	0.027	19.630	0.092	18.169	0.036	-97.3	24.5	HII	4	7.6	1.4	
SK060A	18.561	0.052	20.731	0.104	19.631	0.067	-342.6	17.4	Old	4	

Table 3—Continued

Name	T_1	$\sigma_{T_1}^a$	C^a	σ_C	M^a	σ_M	Velocity (km s ⁻¹)	σ_V (km s ⁻¹)	Type ^b	Ref ^b	R^c	EW (Å)	Notes
SK061A	18.754	0.075	19.823	0.050	18.904	0.040	-179.8	31.3	Old	4	0.0	0.0	
SK062A	19.081	0.060	20.525	0.143	19.670	0.073	-134.1	18.9	Old	4	
SK063A	17.644	0.026	20.095	0.056	18.680	0.031	-242.8	14.0	Star	4	
SK064A	19.305	0.051	20.938	0.095	19.840	0.052	-35.0	16.1	Old	4	
SK065A	18.094	0.041	19.354	0.032	18.749	0.034	-152.5	42.0	Star	4	
SK066A	19.808	0.198	20.989	0.142	20.645	0.192	-180.1	52.0	Old	4	
SK067A	17.988	0.036	20.237	0.065	19.011	0.042	-167.6	36.1	Galaxy	3	Probable M31 cluster ⁱ
SK068A	19.083	0.041	21.031	0.101	19.866	0.052	-330.6	36.5	Young	2	
SK069A	18.222	0.046	19.681	0.042	19.159	0.049	-192.5	12.3	Star	4	
SK070A	18.485	0.057	20.855	0.112	19.462	0.063	-97.3	21.6	Galaxy	3	12.0	13	Probable M31 cluster ⁱ
SK071A	18.760	0.073	21.380	0.178	19.778	0.083	-133.4	17.3	Old	3	
SK072A	16.973	0.012	18.799	0.016	17.809	0.012	-148.0	16.5	Old	4	1.1	0.3	
SK073A	17.507	0.019	19.431	0.027	18.403	0.020	-436.4	10.7	Old	4	
SK074A	18.375	0.053	19.938	0.053	19.198	0.050	-204.1	22.9	Star	4	
SK075A	18.873	0.083	20.372	0.079	19.765	0.085	Galaxy	3	$z = 0.074$ galaxy ^h
SK076A	18.343	0.051	19.989	0.055	19.266	0.053	-186.1	96.5	Star	4	
SK077A	17.813	0.025	19.190	0.023	18.446	0.021	-209.0	39.1	Star	4	
SK078A	17.687	0.028	19.078	0.025	18.508	0.027	-179.6	35.1	Galaxy	3	Probable M31 cluster ⁱ
SK079A	18.025	0.038	20.200	0.063	19.179	0.048	-75.4	22.3	Star	3	1.7	0.7	
SK080A	18.070	0.024	19.437	0.053	18.432	0.024	-140.5	23.1	Star	4	
SK081A	18.676	0.041	20.997	0.203	19.719	0.074	-161.2	14.3	Star	4	
SK082A	19.327	0.075	20.704	0.170	19.926	0.093	-135.9	31.5	Star	4	> 1.5	1.0	
SK083A	19.027	0.056	21.215	0.251	20.267	0.121	-153.2	14.2	Old	4	
SK084A	18.192	0.036	19.243	0.025	18.983	0.034	-232.7	32.1	(Young)	...	1.1	1.7	
SK085A	18.419	0.056	19.301	0.032	19.192	0.051	-66.4	40.7	Star	4	
SK086A	17.243	0.018	19.376	0.030	18.138	0.019	-76.6	16.3	Old	4	
SK087A	18.084	0.024	19.389	0.051	18.889	0.036	-112.6	16.4	Star	4	
SK088A	18.482	0.033	21.951	0.438	19.552	0.061	-137.0	42.0	Star	4	
SK089A	18.812	0.077	21.061	0.138	19.821	0.087	-120.4	28.8	Star	4	
SK090A	18.915	0.087	20.219	0.070	19.633	0.076	-178.0	24.7	(Old)	
SK091A	18.338	0.030	19.839	0.076	19.553	0.064	-113.1	44.9	Star	4	> 1.0	0.6	
SK092A	19.299	0.074	20.349	0.126	19.799	0.084	-67.2	23.4	(Young)	
SK093A	18.940	0.053	20.445	0.132	19.868	0.087	-102.2	25.9	Old	4	
SK094A	18.160	0.043	19.607	0.040	18.934	0.040	-157.8	20.7	Star	3	0.5	1.0	

Table 3—Continued

Name	T_1	σ_{T_1} ^a	C^a	σ_C	M^a	σ_M	Velocity (km s ⁻¹)	σ_V (km s ⁻¹)	Type ^b	Ref ^b	R^c	EW (Å)	Notes
SK095A	18.741	0.044	20.518	0.138	19.859	0.085	-77.4	30.4	(Old)	
SK096A	17.942	0.029	19.269	0.025	18.567	0.023	-54.6	8.6	Star	4	
SK097A	18.521	0.061	19.748	0.046	19.120	0.048	-139.8	45.9	(Old)	
SK098A	18.553	0.062	19.914	0.052	19.390	0.060	-141.6	16.6	Star	4	0.9	5.0	
SK099A	18.300	0.030	19.435	0.054	18.917	0.037	-111.9	39.7	Star	4	
SK100A	18.236	0.046	19.805	0.047	19.130	0.047	-166.3	11.9	Star	4	
SK100C	(17.963)	...	(20.934)	...	(19.135)	...	-486.3	29.2	(Old)	
SK101A	18.795	0.045	20.564	0.125	19.675	0.068	-76.2	18.2	Star	4	
SK104A	17.367	0.012	19.109	0.033	18.284	0.019	-171.1	9.6	Old	4	0.0	0.0	
SK105A	18.497	0.034	19.997	0.076	19.201	0.045	-135.6	17.0	(Old)	
SK106A	18.939	0.051	20.768	0.150	19.960	0.088	-157.8	30.9	Star	4	
V014	(17.052)	...	(18.113)	...	(17.519)	...	-489.2	55.8	Young	3	
V031	17.450	0.016	18.628	0.015	18.142	0.013	-457.5	30.7	Young	1	
V034	16.475	0.016	17.398	0.015	17.969	0.031	HII	3	$z = 0.017$ galaxy ^h
V202	-487.0	48.7	Young	3	
VDB0-B195D	14.889	0.002	15.184	0.001	15.220	0.001	-561.5	48.3	Young	1	
V202 (pos?)	18.804	0.047	20.646	0.086	20.714	0.140	Young	3	1.8	66	
Ma94a(380)	14.720	-31.4	6.7	0.0	0.066	
MIT311	18.340	-113.0	28.0	1.8	0.866	

^aNumbers in parenthesis have been transformed into the Washington system using literature *BVI* measurements and the relations of Bessell (2001).

^bThe cluster age/type classification has been adopted from the following references: (1) Strader et al. (2011); (2) Caldwell et al. (2011); (3) Caldwell et al. (2009); (4) Peacock et al. (2010)

^cDerived ratio of [O III] to $H\beta$ using the procedures described in § 2

^dClassified on the basis of an emission line a 5046 Å.

^eClassified on the basis of a 50 Å FWHM logarithmic-profile emission line at 4836 Å.

^fClassified on the basis of weak emission at 4548 Å.

^gBoth [O III] $\lambda 5007$ and $H\beta$ are well resolved and have the same double-peaked emission profile.

^hClassified using the redshifted emission lines of $H\beta$ and the [O III] doublet.

ⁱClassified as a galaxy in the literature, but our spectrum is consistent with the object being a star cluster.

Table 4. Clusters with Candidate Planetary Nebulae

Cluster	Age (Gyr) ^a	M_V	S/N (5007 Å)	S/N (H β)	R^b	EW (Å)	M_{5007}	Δv (km s ⁻¹)	$\Delta v/\sigma_{\text{eff}}$
Globular Clusters									
B115-G177	14	-8.54	72	16	3.0	2.5	-2.0	-5	0.42
BH16	Old	-6.46	8.3	2.4	4.0	0.7	+0.7	-19	2.71
NB89 ^c	10.4	-6.60	36	12	2.1	1.5	+0.5	-34	1.10
Young Clusters									
B458-D049	0.5	-6.73	6.0	1.6	2.1	0.8	+0.9	+18	2.87
M040	Young	-4.98	5.5	1.1	4.1	1.6	+1.5	+24	0.91
C009-LGS04131	0.3	-5.58	6.3	...	> 6.0	1.0	+1.8	+10	0.32 ¹
SK018A	0.8	-5.09	7.0	...	> 4.0	1.2	+1.9	+8	0.50 ⁵³
DAO47	0.5	-5.52	3.8	...	3.5	0.5	+2.3	+9	0.79 ¹
Possible Clusters									
SK044A	“Star”	-5.36	15	...	> 12	1.9	+1.5	+59	0.12
SK051A	“Star”	-4.40	6.5	...	> 5.0	1.5	+2.3	-33	1.45
Milky Way Clusters									
Pal 6/JaFu1	Old	-6.79	6.3	...	-3.3	-25	0.29
M15/Ps 1	Old	-9.19	2.0	...	+0.7	+23	1.35
NGC 6441/JaFu2	Old	-9.63	3.3	...	+2.8	-21	1.06
M22/GJJC-1	Old	-8.50	> 50	...	+5.1	-16	1.14

^aAge estimate of Caldwell et al. (2009, 2011); Objects labeled as “Star” were classified by Peacock et al. (2010).

^bRatio of [O III] to $H\beta$

^cAge from Beasley et al. (2005); emission may be warm ISM